

Department of Physics and Astronomy
University of Heidelberg

Bachelor Thesis in Physics
submitted by

Bastian Brunner

born in Sinsheim (Germany)

2021

Electron Dynamics Controlled via Radiation Reaction

This Bachelor Thesis has been carried out by Bastian Brunner at the
Max Planck Institute for Nuclear Physics in Heidelberg
under the supervision of
Honorarprofessor Dr. Christoph H. Keitel

Abstract

If a charge is hit by a superstrong laser pulse, such as those that can be created with state-of-the-art laser technology, it experiences an extreme acceleration causing the motion of the charge to be strongly affected by its own emission of radiation. In classical electrodynamics this effect can be taken into account by adding a new force term (also called radiation reaction) to the equation of motion of the charge in addition to the Lorentz force. Here we show how the radiation reaction force can be used to control the deflection of a relativistic beam of electrons colliding head-on with a plane-wave laser pulse as well as in the head-on and oblique incidence collision with a tightly focused laser pulse. In addition, strong-field QED effects are also considered by correcting the classical radiation reaction force with a quantum factor, leading to a semiclassical treatment. All of this is done by performing analytic calculations and by numerical integration with a fourth order Runge-Kutta method, which is tested against the analytic result of the plane wave case.

Zusammenfassung

Wird eine Ladung von einem hochenergetischem Laserpuls getroffen, wie er mit modernster Lasertechnik erzeugt werden kann, erfährt sie eine extreme Beschleunigung, so dass die Bewegung der Ladung durch ihre eigene Strahlungsemission stark beeinflusst wird. In der klassischen Elektrodynamik kann dieser Effekt berücksichtigt werden, indem zusätzlich zur Lorentz-Kraft ein neuer Kraftterm (auch Strahlungsrückwirkung genannt) in die Bewegungsgleichung für die Ladung aufgenommen wird. Hier wird gezeigt, wie die Strahlungsrückwirkungskraft genutzt werden kann, um die Ablenkung eines relativistischen Elektronenstrahls zu kontrollieren, der frontal mit einer ebenen Welle kollidiert, sowie frontal und senkrecht mit einem stark fokussierten Laserpuls kollidiert. Darüber hinaus werden QED-Effekte berücksichtigt, indem die klassische Strahlungsrückwirkungskraft mit einem Quantenfaktor korrigiert wird, was zu einer semiklassischen Beschreibung führt. All dies geschieht durch analytische Berechnungen und durch numerische Integration mit einer Runge-Kutta-Methode vierter Ordnung, die mit dem analytischen Ergebnis der ebenen Welle überprüft werden kann.

Contents

1	Introduction	5
1.1	The Lorentz-Abraham-Dirac equation	6
1.2	The Landau-Lifschitz equation	7
1.3	Quantum effects	8
1.4	Structure of this thesis	9
2	Plane-wave laser pulse	10
2.1	Classical solution of the LL equation for a plane wave	10
2.2	Semiclassical solution of the LL equation for a plane wave	13
2.3	Physical application	16
2.4	Analytics of a single electron	17
2.5	The numerical integrator	22
2.6	Numerical analysis of a single electron	23
2.7	Simulation of an electron beam	27
3	Tightly focused laser pulse	33
3.1	Field components and geometry	33
3.2	Head-on collision	35
3.3	Oblique incidence collision	39
4	Conclusion	44
5	Mathematical appendix	45
5.1	Picard iteration for the classical solution	45
5.2	Picard iteration for the semiclassical solution	47
5.3	Identities and integrals	48
6	Bibliography	49
7	Acknowledgements	52

1 Introduction

Laser technology has made significant progress in the last decades. Laser pulses with femtosecond duration (10^{-15} s) have reached a record intensity of $2 \cdot 10^{22} \text{W/cm}^2$ in the laser pulse focal area [1]. Further, many facilities around the world are developing 10-PW-class laser systems such as the research infrastructure APOLLON [2] in France and the Extreme-Light-Infrastructure (ELI) [3] which is designed to reach an intensity of $10^{23} - 10^{24} \text{W/cm}^2$. The applications of the experimental research available at these scales range from testing fundamental physics to life sciences. A fundamental understanding of the forces that dominate physics in this superstrong field regime is therefore essential.

An electron hit by this kind of laser pulse experiences extremely high accelerations and becomes ultrarelativistic within one laser period. As every accelerated charge emits electromagnetic radiation, one can expect the electron's motion to be strongly influenced by energy loss due to radiation, leading the electron to be influenced by its own radiation. This effect needs to be considered in the equation of motion of the particle. In classical electrodynamics, this is referred to as the radiation reaction (RR) force. The typical equation of motion for a non-relativistic particle with charge q and mass m_q considering only the Lorentz force is (in Gaussian units)

$$\frac{d\mathbf{p}}{dt} = \mathbf{F}_{Lorentz} = q \left(\mathbf{E} + \frac{\mathbf{v}}{c} \times \mathbf{B} \right), \quad (1.1)$$

where $\mathbf{v} = \mathbf{p}/m_q$ is the particle's velocity, $c \approx 3 \cdot 10^8 \text{m/s}$ is the speed of light and \mathbf{E}, \mathbf{B} are the electromagnetic fields, respectively. The RR force can be introduced as an additional term resulting in

$$\dot{\mathbf{p}} = \mathbf{F}_{Lorentz} + \mathbf{F}_{RR}. \quad (1.2)$$

An intuitive way to understand the additional RR force term has been shown by Jackson [4]. He derived the RR force term by identifying the energy radiated away according to Larmor's formula in a given time interval with the work acting on the

particle due to the RR force during that interval.

$$E_{lost} = \int_{t_0}^{t_1} P_{Larmor} dt = \int_{t_0}^{t_1} \frac{2q^2}{3c^3} \left(\frac{d\mathbf{v}}{dt} \right)^2 dt \equiv \int_{t_0}^{t_1} \mathbf{F}_{RR} \cdot \mathbf{v} dt. \quad (1.3)$$

After partial integration and with the condition that $\mathbf{v} \cdot \frac{d\mathbf{v}}{dt}$ vanishes at the boundaries of the chosen time interval one can identify the RR-force by

$$\mathbf{F}_{RR} = \frac{2q^2}{3c^3} \frac{d^2\mathbf{v}}{dt^2}. \quad (1.4)$$

From the theoretical point of view, the problem of radiation reaction has been studied long before the access to current high energetic setups, even before the realisation of lasers. The formula (1.4) shown here has already been derived by Abraham and Lorentz in 1905 [5]. It is important to note that it depends on the derivative of the acceleration. This leads to several problems, for example, even with no external field, the equation (1.2) has a solution that exponentially accelerates the charge [4] [6].

1.1 The Lorentz-Abraham-Dirac equation

As the RR force only becomes relevant at velocities close to the speed of light, it is necessary to have a relativistic generalisation of the force (1.4). This has been achieved by P. Dirac in 1938 [7] and is called the Lorentz-Abraham-Dirac (LAD) equation

$$m_q \frac{du^\mu}{ds} = \frac{q}{c} F^{\mu\nu} u_\nu + \frac{2q^2}{3c^3} \left(\frac{d^2 u^\mu}{ds^2} + \frac{du^\nu}{ds} \frac{du_\nu}{ds} u^\mu \right), \quad (1.5)$$

where $F^{\mu\nu}(x)$ is the electromagnetic field tensor of the external field (without the self-induced field), $u^\mu = dx^\mu/ds = (\gamma, \gamma\mathbf{v}/c)$ is the four velocity and s is the proper time. From here on Greek indices denote four vectors with $\mu, \nu, \dots = \{0, 1, 2, 3\}$ and the Einstein notation for summation over same indices is used. The first term on the right hand side of the equation expresses the Lorentz force, while the other one describes the interaction of the particle with its own radiation. The additional term in the latter proportional to u^μ can be understood intuitively by demanding that for any four force f^μ the condition $u_\mu f^\mu = 0$ must be satisfied which is valid for the following

$$u_\mu \left(\frac{d^2 u^\mu}{ds^2} - u^\mu u_\nu \frac{d^2 u^\nu}{ds^2} \right) = u_\mu \frac{d^2 u^\mu}{ds^2} - \underbrace{u_\mu u^\mu}_{=1} u_\nu \frac{d^2 u^\nu}{ds^2} = 0, \quad (1.6)$$

because of the "on the mass shell" condition $u_\mu u^\mu = 1$. With the identity

$$\frac{d}{ds} \left(u_\nu \frac{du^\nu}{ds} \right) = 0 = \frac{du^\nu}{ds} \frac{du_\nu}{ds} + u_\nu \frac{d^2 u^\nu}{ds^2}, \quad (1.7)$$

the reason for the structure of (1.5) becomes immediately clear. The problem of non-physical solutions occurs in the LAD equation as well, and there is much discussion about its validity [8] [9].

1.2 The Landau-Lifschitz equation

One way to solve the problem of non-physical solutions has been shown by L. Landau and D. Lifschitz in 1975 by perturbative reduction [6]. They considered the self-force to be small compared to the Lorentz force in the rest frame of the charge and because of the Lorentz invariant nature of the LAD equation this assumption also holds true in other frames of reference. Then one can treat the self-force as a perturbative effect with the following zero order expression

$$\frac{du^\mu}{ds} = \frac{q}{m_q c} F^{\mu\nu} u_\nu, \quad (1.8)$$

for the derivative of the four velocity. Since the RR force term will be approximated, the expression will only be substituted into the right hand side of the LAD equation (1.5) to get to the Landau-Lifschitz (LL) equation

$$\begin{aligned} \frac{du^\mu}{ds} = & \frac{q}{m_q c} F^{\mu\nu} u_\nu + \frac{2}{3} \left(\frac{q^3}{m_q^2 c^3} (\partial_\alpha F^{\mu\nu}) u^\alpha u_\nu + \frac{q^4}{m_q^3 c^5} F^{\mu\nu} F_{\alpha\nu} u^\alpha \right. \\ & \left. + \frac{q^4}{m_q^3 c^5} (F^{\alpha\nu} u_\nu) (F_{\alpha\beta} u^\beta) u^\mu \right). \end{aligned} \quad (1.9)$$

According to Landau and Lifschitz, the case of the RR force being small compared to the Lorentz force in the rest frame is a condition for the equation of motion $\dot{\mathbf{p}} = \mathbf{F}_{Lorentz} + \mathbf{F}_{RR}$ to be valid [6]. Using this equation for an electron in the frame where $\mathbf{v} = 0$ the derivative of the acceleration becomes

$$\ddot{\mathbf{v}} = \frac{e}{m} \dot{\mathbf{E}} + \frac{e}{mc} (\dot{\mathbf{v}} \times \mathbf{B}) = \frac{e}{m} \dot{\mathbf{E}} + \frac{e^2}{m^2 c} (\mathbf{E} \times \mathbf{B}), \quad (1.10)$$

if the \mathbf{F}_{RR} term is neglected. Here $e > 0$ is defined as the absolute value of the charge of an electron and m denotes the electron mass. For a periodic motion with

frequency $\omega = c/\lambda$ the temporal derivative of the field gives $\dot{\mathbf{E}} \propto \omega \mathbf{E}$ and therefore

$$\mathbf{F}_{RR} \propto \frac{2e^3}{3mc^2\lambda} \mathbf{E} + \frac{2e^4}{3m^2c^4} (\mathbf{E} \times \mathbf{B}) \underbrace{\ll}_{\text{condition}} \mathbf{F}_{Lorentz} = e\mathbf{E}. \quad (1.11)$$

Demanding that this force is small compared to the Lorentz force one finds from the two terms of \mathbf{F}_{RR} in equation (1.11) the following two independent conditions:

a) The change in the field amplitude needs to happen on scales much larger than the classical electron radius $r_e = e^2/mc^2 \approx 2.8 \cdot 10^{-15}m$.

b) The field strengths involved must not exceed the value of a classical critical field given by $F_c = m^2c^4/e^3 \approx 1.8 \cdot 10^{20} \frac{V}{m}$.

1.3 Quantum effects

Both of the two conditions above are satisfied in the classical framework because of quantum effects becoming relevant before reaching the two limiting conditions above. Approaching the point limit the Compton wavelength sets an earlier limit with $\lambda_C = \hbar/mc \approx 3.9 \cdot 10^{-13}m$, while the critical field of quantum electrodynamics (QED) with $F_q = m^2c^3/e\hbar \approx 1.3 \cdot 10^{18} \frac{V}{m}$ is smaller than F_c by a factor of $\alpha \approx 1/137$. Quantum effects are observations that cannot be explained by classical electrodynamics but follow directly from the QED, such as the spin force, pair production and the stochasticity of photon emission. The theory of QED has been developed in the 1940s and treats charged point particles as excitations in a field with quantised energy and momentum [10]. The LAD equation and the LL equation both are purely classical so it is important to have an estimation of their validity with increasing quantum effects. The quantum nonlinearity parameter

$$\chi \equiv \frac{|e|\hbar}{m^3c^4} \sqrt{|F^{\mu\nu}p_\nu|^2} = \frac{|e|\hbar}{m^3c^4} \sqrt{(\mathbf{E} \cdot \mathbf{p})^2 - (\mathbf{E} \cdot \gamma mc + \mathbf{B} \times \mathbf{p})^2}, \quad (1.12)$$

expresses the strength of quantum effects and one finds the LL equation to be valid if the condition $\chi \ll 1$ holds true [11]. Here $\hbar = h/2\pi \approx 1.055 \cdot 10^{-34}Js$ is the reduced Planck constant.

The only quantum correction that is considered in this thesis is to account for the reduced emission of radiation and is implemented by a weighting factor multiplying the RR term in the LL equation (1.9) (see section 2.33 for more details).

1.4 Structure of this thesis

From equation (1.11) it becomes clear that the strength of the RR force depends mainly on the charge to mass ratio, therefore electrons are most affected by this force. Their dynamics under the influence of superstrong laser pulses will be investigated. At first the solution of the LL equation for a plane wave will be derived analytically, similar to Reference [12]. In addition, this will be done again for a quantum corrected LL equation. In the next step, the results will be used to test a numerical integrator and validate its functionality for a plane wave. This will also be done in the case of a relativistic electron beam instead of a single electron, following the ideas put forward in Reference [13]. From there, knowing that the integrator works properly, it will be used to investigate the influence of a tightly focused laser pulse, where an analytic solution is unavailable.

2 Plane-wave laser pulse

From here on, natural units $\hbar = c = 1$ are used, the fine-structure constant is taken as $\alpha = e^2/4\pi \approx 1/137$. The space-time coordinates are denoted as $x^\mu = (ct, \mathbf{x})$ and the Minkowski metric with $\eta^{\mu\nu} = \text{diag}(1, -1, -1, -1)$ is used. With this metric, the square of a four vector is defined as $a^2 \equiv \eta_{\mu\nu} a^\mu a^\nu = a^\mu a_\mu$.

2.1 Classical solution of the LL equation for a plane wave

In this section the solution of the Landau-Lifschitz equation for a plane wave is presented similar to Reference [12] but in more detail.

A plane wave that is propagating in \mathbf{n} direction can be completely described as a function depending only on the phase $\phi = n_\mu x^\mu$ with $n^\mu = (1, \mathbf{n})$ and $\mathbf{n}^2 = 1$. The aim in the following calculations is to rewrite the LL equation (1.9) in dependence of the phase as it is easier to solve that way.

Expressing the LL equation by the phase The four-vector potential of a plane wave with arbitrary polarization is given by

$$A^\mu = a_1^\mu \Psi_1(\phi) + a_2^\mu \Psi_2(\phi). \quad (2.1)$$

with the constant amplitude four-vector a_j^μ that is chosen so that $a_i^\mu a_{j,\mu} = a_i^2 \delta_{ij}$ and $n_\mu a_i^\mu = 0$ is satisfied for $i, j = \{1, 2\}$. The shape of the pulse will be determined by the arbitrary scalar functions $\Psi_i(\phi)$ depending only on the phase ϕ .

The electromagnetic field tensor $F^{\mu\nu}(\phi) = \partial^\mu A^\nu(\phi) - \partial^\nu A^\mu(\phi)$ then is

$$F^{\mu\nu}(\phi) = \partial^\mu (a_1^\nu \Psi_1(\phi) + a_2^\nu \Psi_2(\phi)) - \partial^\nu (a_1^\mu \Psi_1(\phi) + a_2^\mu \Psi_2(\phi)) \quad (2.2)$$

$$= f_1^{\mu\nu} \Psi_1'(\phi) + f_2^{\mu\nu} \Psi_2'(\phi), \quad (2.3)$$

where the new amplitude tensor $f_j^{\mu\nu} \equiv n^\mu a_j^\nu - n^\nu a_j^\mu = \text{constant}$ has been defined and where a prime denotes derivation by ϕ . It is clear that $n_\mu f_j^{\mu\nu} = 0$ because $n^2 = 0$.

The following identity will become important later

$$f_{i,\mu\nu}f_j^{\beta\nu} = (n_\mu a_{i,\nu} - n_\nu a_{i,\mu})(n^\beta a_j^\nu - n^\nu a_j^\beta) = a_i^2 \delta_{ij} n_\mu n^\beta, \quad (2.4)$$

In order to express the LL equation (1.9) in terms of the phase, equation (1.9) is multiplied by n_μ which gives

$$m \frac{du^\mu}{ds} \cdot n_\mu = - \underbrace{e F^{\mu\nu} u_\nu n_\mu}_{=0} - \frac{2}{3} \alpha \left(\underbrace{\frac{e}{m} (\partial_\alpha F^{\mu\nu}) u^\alpha u_\nu n_\mu}_{=0} + \underbrace{\frac{e^2}{m^2} F^{\mu\nu} F_{\alpha\nu} u^\alpha n_\mu}_{=0} - \frac{e^2}{m^2} (F^{\alpha\nu} u_\nu)(F_{\alpha\beta} u^\beta) u^\mu n_\mu \right) \quad (2.5)$$

$$= \frac{e^2}{m^2} \frac{2}{3} \alpha \left((f_1^{\alpha\nu} \Psi'_1 + f_2^{\alpha\nu} \Psi'_2) u_\nu (f_{1,\alpha\beta} \Psi'_1 + f_{2,\alpha\beta} \Psi'_2) u^\beta u^\mu n_\mu \right), \quad (2.6)$$

because of the orthogonality relation $n_\mu F^{\mu\nu} = 0$. With the identity (2.4) shown above this expression simplifies to

$$m \frac{du^\mu}{ds} \cdot n_\mu = \frac{e^2}{m^2} \frac{2}{3} \alpha (a_1^2 n^\nu n_\beta (\Psi'_1)^2 + a_2^2 n^\nu n_\beta (\Psi'_2)^2) u_\nu u^\beta u^\mu n_\mu \quad (2.7)$$

$$= -\frac{2}{3} \alpha (\xi_1^2 (\Psi'_1)^2 + \xi_2^2 (\Psi'_2)^2) \left(\frac{d\phi}{ds} \right)^3 = m \frac{d^2\phi}{ds^2}. \quad (2.8)$$

Here the ξ_i have been defined as

$$\xi_i^2 \equiv -\frac{a_i^2 e^2}{m^2}, \quad (2.9)$$

with $i = \{1, 2\}$. Multiplying equation (2.8) by $d^2s/d\phi^2$ and using relation (5.22 in appendix) one finds a rather simple ordinary equation for the second derivative of the proper time

$$m \frac{d^2s}{d\phi^2} = \frac{2}{3} \alpha (\xi_1^2 (\Psi'_1)^2 + \xi_2^2 (\Psi'_2)^2). \quad (2.10)$$

Integrating this equation by ϕ with the definition of $\rho(\phi) \equiv n^\mu u_\mu(\phi)$, also called the *Doppler factor*, gives

$$m \int_{\phi_0}^{\phi} \frac{d^2s}{d\Phi^2} d\Phi = m \left(\frac{1}{\rho(\phi)} - \frac{1}{\rho_0} \right) = \frac{2}{3} \alpha \int_{\phi_0}^{\phi} (\xi_1^2 (\Psi'_1(\Phi))^2 + \xi_2^2 (\Psi'_2(\Phi))^2) d\Phi. \quad (2.11)$$

With the initial velocity $u_0^\mu \equiv u^\mu(\phi_0)$ and the corresponding initial Doppler factor $\rho_0 \equiv n^\mu u_{0,\mu}$ this equation simplifies to

$$\rho(\phi) = \frac{\rho_0}{h(\phi)}, \quad (2.12)$$

with

$$h(\phi) \equiv 1 + \frac{2}{3}\alpha \frac{\rho_0}{m} \int_{\phi_0}^{\phi} (\xi_1^2(\Psi'_1(\Phi))^2 + \xi_2^2(\Psi'_2(\Phi))^2) d\Phi. \quad (2.13)$$

This $h(\phi)$ is used to express the reduced four-velocity as $\tilde{u}^\mu \equiv h(\phi)u^\mu(\phi)$. Together with the electromagnetic field tensor of a plane wave the LL equation (1.9) can be expressed in a more simple way. The left-hand side of the LL equation will be

$$\frac{du^\mu(\phi)}{ds} = \frac{d\phi}{ds} \frac{d}{d\phi} \left(\frac{\tilde{u}^\mu(\phi)}{h(\phi)} \right) = \rho(\phi) \left(-\tilde{u}^\mu \frac{dh}{d\phi} \frac{1}{h^2} + \frac{1}{h} \frac{d\tilde{u}^\mu}{d\phi} \right), \quad (2.14)$$

while the right-hand side will give

$$\begin{aligned} m \frac{du^\mu(\phi)}{ds} &= -eF^{\mu\nu} \frac{\tilde{u}_\nu}{h(\phi)} - \frac{2}{3}\alpha \left(\frac{e}{m} \frac{\partial\phi}{\partial x^\alpha} \frac{\partial F^{\mu\nu}}{\partial\phi} u^\alpha \frac{\tilde{u}_\nu}{h(\phi)} + \frac{e^2}{m^2} F^{\mu\nu} F_{\alpha\nu} u^\alpha \right. \\ &\quad \left. - \frac{e^2}{m^2} (F^{\alpha\nu} u_\nu)(F_{\alpha\beta} u^\beta) \frac{\tilde{u}^\mu}{h(\phi)} \right) \end{aligned} \quad (2.15)$$

$$\begin{aligned} &= -eF^{\mu\nu} \frac{\tilde{u}_\nu}{h(\phi)} - \frac{2}{3}\alpha \left(\frac{e}{m} n_\alpha F'^{\mu\nu} u^\alpha \frac{\tilde{u}_\nu}{h(\phi)} + \frac{e^2}{m^2} (a_1^2(\Psi'_1)^2 \right. \\ &\quad \left. + a_2^2(\Psi'_2)^2) n^\mu n_\alpha u^\alpha - \frac{e^2}{m^2} (a_1^2(\Psi'_1)^2 + a_2^2(\Psi'_2)^2) n^\nu n_\beta u_\nu u^\beta \frac{\tilde{u}^\mu}{h(\phi)} \right) \end{aligned} \quad (2.16)$$

$$\begin{aligned} &= -eF^{\mu\nu} \frac{\tilde{u}_\nu}{h(\phi)} - \frac{2}{3}\alpha \left(\frac{e}{m} F'^{\mu\nu} \rho(\phi) \frac{\tilde{u}_\nu}{h(\phi)} - (\xi_1^2(\Psi'_1)^2 + \xi_2^2(\Psi'_2)^2) n^\mu \rho(\phi) \right. \\ &\quad \left. + (\xi_1^2(\Psi'_1)^2 + \xi_2^2(\Psi'_2)^2) \rho^2(\phi) \frac{\tilde{u}^\mu}{h(\phi)} \right). \end{aligned} \quad (2.17)$$

By comparing the first term of equation (2.14) to the last term in (2.17) one can see that these terms cancel out. Using the relation $\rho(\phi) = \rho_0/h(\phi)$ the LL equation becomes

$$m \frac{d\tilde{u}^\mu(\phi)}{d\phi} = -\frac{\tilde{u}_\nu}{\rho_0} \left(h(\phi) e F^{\mu\nu} + \frac{2}{3}\alpha \frac{e}{m} F'^{\mu\nu} \rho_0 \right) + n^\mu \frac{2}{3}\alpha h(\phi) (\xi_1^2(\Psi'_1)^2 + \xi_2^2(\Psi'_2)^2). \quad (2.18)$$

Solving the LL equation The differential equation (2.18) with the only parameter being the phase ϕ can be solved by Picard iteration (see 5.1 in appendix for more details). The solution obtained by the iteration is for \tilde{u}^μ , so for the four-velocity u^μ one finds instead

$$\begin{aligned} u^\mu(\phi) &= \frac{1}{h(\phi)} \left(u_0^\mu - \frac{e}{\rho_0 m} (f_1^{\mu\nu} I_1(\phi) + f_2^{\mu\nu} I_2(\phi)) u_{0,\nu} + \frac{1}{2\rho_0} (h^2(\phi) - 1) n^\mu \right. \\ &\quad \left. + \frac{1}{2\rho_0} (\xi_1^2 I_1^2(\phi) + \xi_2^2 I_2^2(\phi)) n^\mu \right). \end{aligned} \quad (2.19)$$

The following integral has been defined

$$I_j(\phi) \equiv \int_{\phi_0}^{\phi} \left(h(\Phi) \Psi_j'(\Phi) + \frac{2}{3} \alpha \frac{\rho_0}{m} \Psi_j''(\Phi) \right) d\Phi. \quad (2.20)$$

The space-time coordinates depending on the phase are then given by

$$x^\mu(\phi) = x_0^\mu + \frac{1}{\rho_0} \int_{\phi_0}^{\phi} h(\Phi) u^\mu(\Phi) d\Phi, \quad (2.21)$$

with $x^\mu(\phi_0) \equiv x_0^\mu$ and because of the following relation:

$$x^\mu - x_0^\mu = \int_{\tau_0}^{\tau} \frac{dx^\mu}{ds} ds = \int_{\phi_0}^{\phi} \frac{dx^\mu}{ds} \frac{ds}{d\Phi} d\Phi = \int_{\phi_0}^{\phi} u^\mu(\Phi) \frac{h(\Phi)}{\rho_0} d\Phi. \quad (2.22)$$

By looking at equation (2.19) one notices that the only contribution of the derivative of the fields term in the LL equation (1.9) happens to be in the integral (2.20). It can also be seen that it averages out for periodic Ψ_j as all other factors remain constant. Later it will be shown that the term can even be neglected completely.

2.2 Semiclassical solution of the LL equation for a plane wave

Classical electrodynamics does not account for the fact that an electron cannot produce photons exceeding its kinetic energy. It becomes apparent that the classical solution overestimates the radiation produced by the moving charge, and that the equations need to be changed to implement this quantum cut-off. Therefore one introduces a scalar function

$$g(\chi) \equiv \frac{I_q}{I_c} = \frac{1}{I_c} \frac{e^2 m^2}{3\sqrt{3}\pi} \int_0^\infty \frac{u(4u^2 + 5u + 4)}{(1+u)^4} K_{2/3} \left(\frac{2u}{3\chi} \right) du, \quad (2.23)$$

with I_q being the quantum radiation intensity, $I_c = 2e^2 m^2 \chi^2 / 3$ the classical radiation intensity and $K_{2/3}(\cdot)$ the modified Bessel function of order 2/3 [14]. The quantum parameter χ is defined as

$$\chi = \frac{|e|}{m^3} \sqrt{|F^{\mu\nu} p_\nu|^2}, \quad (2.24)$$

and represents the strength of quantum effects. For $\chi \ll 1$ quantum effects can be neglected in the LL equation while for $\chi \approx 1$ they become dominant [11]. A good

approximation for this expression (2.23) is presented in reference [14] and is

$$g(\chi) \approx (1 + 4.8(1 + \chi) \ln(1.7\chi) + 2.44\chi^2)^{-\frac{2}{3}}, \quad (2.25)$$

which approximates equation (2.23) with an accuracy of better than 2% for all quantum parameters [14] [15].

This function will only be relevant for the radiation reaction terms, as these terms reflect the interaction of the particle with its own radiation. The new LAD equation will look like this:

$$m \frac{du^\mu}{ds} = -eF^{\mu\nu}u_\nu + g(\chi)\frac{2}{3}\alpha \left(\frac{d^2u^\mu}{ds^2} + \frac{du^\nu}{ds} \frac{du_\nu}{ds} u^\mu \right). \quad (2.26)$$

The term containing the derivatives of the field in the LL equation (1.9) will be neglected. The reason for this will be discussed in the section below. The resulting equation is

$$m \frac{du^\mu}{ds} = -eF^{\mu\nu}u_\nu - g(\chi)\frac{2}{3}\alpha \left(\frac{e^2}{m^2} F^{\mu\nu} F_{\alpha\nu} u^\alpha - \frac{e^2}{m^2} (F^{\alpha\nu} u_\nu) (F_{\alpha\beta} u^\beta) u^\mu \right). \quad (2.27)$$

It is important to note that $g(\phi) = g(F^{\mu\nu}(\phi), p_\nu(\phi))$ is a function of the fields and the momentum, while both of these quantities depend on the phase as well. However, assuming the change in momentum to be small, the function can be treated as an external-known function of ϕ (like $F^{\mu\nu}$) and can be set constant in the iteration for small phase steps. Certainly, this leads to expressions that cannot be solved exactly but can only be iterated. The term containing the $g(\chi)$ function is proportional to F^2 , so it can be absorbed into the definition of the electromagnetic field tensor

$$\tilde{F}^{\mu\nu}(\phi) \equiv f_1^{\mu\nu} \tilde{\Psi}'_1(\phi) + f_2^{\mu\nu} \tilde{\Psi}'_2(\phi) \equiv f_1^{\mu\nu} \sqrt{g(\phi)} \Psi'_1(\phi) + f_2^{\mu\nu} \sqrt{g(\phi)} \Psi'_2(\phi). \quad (2.28)$$

With this definition the calculations can be done equivalently to section 2.1, with respect to $\tilde{F}^{\mu\nu}(\phi)$ and $\tilde{\Psi}'_j(\phi)$ instead of $F^{\mu\nu}(\phi)$ and $\Psi'_j(\phi)$ up to equation (2.15). One finds instead

$$m \frac{du^\mu(\phi)}{ds} = -e \frac{\tilde{F}^{\mu\nu}}{\sqrt{g(\phi)}} \frac{\tilde{u}_\nu}{\tilde{h}(\phi)} - \frac{2}{3}\alpha \left((\xi_1^2 (\Psi'_1)^2 + \xi_2^2 (\tilde{\Psi}'_2)^2) n^\mu \rho(\phi) + (\xi_1^2 (\tilde{\Psi}'_1)^2 + \xi_2^2 (\tilde{\Psi}'_2)^2) \rho^2(\phi) \frac{\tilde{u}^\mu}{\tilde{h}(\phi)} \right), \quad (2.29)$$

with the $\tilde{h}(\phi)$ in this case being

$$\tilde{h}(\phi) = 1 + \frac{2}{3}\alpha\frac{\rho_0}{m}\int_{\phi_0}^{\phi} g(\Phi)(\xi_1^2(\Psi'_1(\Phi))^2 + \xi_2^2(\Psi'_2(\Phi))^2) d\Phi. \quad (2.30)$$

It follows a new differential equation for $\tilde{u}^\mu(\phi) = \tilde{h}(\phi)u^\mu(\phi)$, namely

$$m\frac{d\tilde{u}^\mu(\phi)}{d\phi} = -\frac{\tilde{u}_\nu}{\rho_0}\tilde{h}(\phi)e\frac{\tilde{F}^{\mu\nu}}{\sqrt{g(\phi)}} + n^\mu\frac{2}{3}\alpha\tilde{h}(\phi)(\xi_1^2(\tilde{\Psi}'_1)^2 + \xi_2^2(\tilde{\Psi}'_2)^2). \quad (2.31)$$

Again, the solution will be obtained using the Picard iteration (see 5.2 in appendix for more details). The following integral has been defined

$$\tilde{I}_j(\phi) \equiv \int_{\phi_0}^{\phi} \tilde{h}(\Phi)\frac{\tilde{\Psi}'_j(\Phi)}{\sqrt{g(\Phi)}} d\Phi = \int_{\phi_0}^{\phi} \tilde{h}(\Phi)\Psi'_j(\Phi) d\Phi. \quad (2.32)$$

The solution for the four velocity in the semiclassical case reads

$$u^\mu(\phi) = \frac{1}{\tilde{h}(\phi)}\left(u_0^\mu - \frac{e}{\rho_0 m}(f_1^{\mu\nu}\tilde{I}_1(\phi) + f_2^{\mu\nu}\tilde{I}_2(\phi))u_{0,\nu} + \frac{1}{2\rho_0}(\tilde{h}^2(\phi) - 1)n^\mu + \frac{1}{2\rho_0}\left(\xi_1^2\tilde{I}_1^2(\phi) + \xi_2^2\tilde{I}_2^2(\phi)\right)n^\mu\right), \quad (2.33)$$

and therefore for the space-time coordinates

$$x^\mu(\phi) = x_0^\mu + \frac{1}{\rho_0}\int_{\phi_0}^{\phi} \tilde{h}(\Phi)u^\mu(\Phi) d\Phi. \quad (2.34)$$

With equations (2.33) and (2.34) one finds the momentum and position given by the two integrals h and I . Instead of deriving an exact solution of the integrals as can be done in the classical case they will be solved by iteration. At a small phase step $\Delta\phi$ the momentum will be calculated by equation (2.33) while the position can be calculated by (2.34) but with the momentum in the equations replaced with the initial momentum. From there, the quantities can be calculated at the next step with the momentum and the position from the previous step.

The same kind of iteration has been done in the classical case for testing and agreement has been found to the purely analytic solution from section 2.1. As can be seen in section 2.7, the analytic values predicted by this iteration match the ones of the numerical simulation.

2.3 Physical application

The following sections are closely related to the original idea put forward in Reference [13]. A plane-wave pulse that is propagating in z-direction with a linear polarisation in x-direction will be chosen. With these conditions the only non-zero field components are E_x and B_y .

The Gaussian unit system introduced above will no longer be used because with the wavelength λ of the laser everything can be expressed in dimensionless quantities. Therefore in the following calculations and simulations time is expressed in units of $\omega^{-1} \equiv \lambda/2\pi c$, length in units of $c\omega^{-1}$, momentum in units of mc and fields in units of $m\omega c/|e|$.

With that the LL equation (1.9) gives for the spatial momentum components expressed in terms of the \mathbf{E} - and \mathbf{B} -field

$$\begin{aligned} \frac{d\mathbf{p}}{dt} = & -(\mathbf{E} + \mathbf{v} \times \mathbf{B}) - \frac{4\pi r_e}{3\lambda} \left(\gamma \left[\left(\frac{\partial}{\partial t} + \mathbf{v} \cdot \nabla \right) \mathbf{E} + \mathbf{v} \times \left(\frac{\partial}{\partial t} + \mathbf{v} \cdot \nabla \right) \mathbf{B} \right] \right. \\ & \left. - [(\mathbf{E} + \mathbf{v} \times \mathbf{B}) \times \mathbf{B} + (\mathbf{v} \cdot \mathbf{E})\mathbf{E}] + \gamma^2 [(\mathbf{E} + \mathbf{v} \times \mathbf{B})^2 - (\mathbf{v} \cdot \mathbf{E})^2] \mathbf{v} \right), \end{aligned} \quad (2.35)$$

where the constant $r_e = e^2/mc^2$ denotes the classical electron radius.

With a wavelength in the optical regime, the constant factor that multiplies the RR force is of the order of 10^{-8} and it becomes clear that intense fields with normalised laser amplitude $\xi \gg 1$ and ultrarelativistic particles with $\gamma \gg 1$ are necessary for the RR force to become noticeable. The last term (γ^2 term) is roughly at a scale of $\gamma^2 \xi^2$ and is therefore the dominating term in the RR force. Because it describes a loss of energy that depends mainly on the velocity, it is referred to as the *friction term* [16]. Analysing the term containing the derivatives of the fields, it is approximately $\gamma \xi$ smaller than the dominating term. Finding this behaviour in addition to the discovery in section 2.1, where it has been shown that the derivative term's contribution averages out for periodic field pulses, one can therefore neglect it completely.

It could be argued that the term without any γ can be neglected as well as its contribution is by a factor of γ^2 smaller than the dominating term, but it will be kept to satisfy the "on the mass shell" condition $u^\mu u_\mu = 1$. This can be seen by multiplying the LL equation (1.9) by u_μ and taking into account that $F^{\mu\nu}$ is anti-symmetric under permutation of the indices.

2.4 Analytics of a single electron

For a better physical understanding of the analytic solution it is helpful to express $h(\phi)$ and $I_j(\phi)$ in terms of the fields. With the identity

$$(\mathbf{E} \times \mathbf{B})_i = -\frac{1}{2}\epsilon_{ijk}F^{0j}\epsilon^{klm}F_{lm} = n_i(a_1^2\Psi_1'^2 + a_2^2\Psi_2'^2), \quad (2.36)$$

it is clear that $h(\phi)$ can be rewritten in the classical case as

$$h(\phi) = 1 + r_R\rho_0 \int_{\phi_0}^{\phi} (\mathbf{E}(\Phi) \times \mathbf{B}(\Phi)) \mathbf{n} d\Phi, \quad (2.37)$$

where the constants have been absorbed into the constant r_R with

$$r_R \equiv \frac{4\pi e^2}{3mc^2\lambda}. \quad (2.38)$$

One can define the vector equation for the integrals derived in section 2.1 as

$$\mathbf{I}(\phi) \equiv - \int_{\phi_0}^{\phi} h(\Phi)\mathbf{E}(\Phi) d\Phi. \quad (2.39)$$

The equation for the momentum can then be found from the three velocity components of equation (2.19)

$$\mathbf{p} = \frac{\mathbf{p}_0 + \mathbf{I}}{h} + \frac{2\mathbf{I} \cdot \mathbf{p}_0 + (h^2 - 1) + \mathbf{I}^2}{2\rho_0 h} \mathbf{n}. \quad (2.40)$$

After the laser-electron interaction, the electron the momentum will not change anymore and therefore the change in momentum caused by the laser pulse can be calculated by only considering the final values of $\mathbf{I}_f \equiv \mathbf{I}(\phi_f)$ and $h_f \equiv h(\phi_f)$.

For an electron that is counter propagating to a plane-wave pulse, the transverse momentum gain will be happening in the x-direction as the only non zero components of the electric field are $E_x = B_y$. With an initial momentum of $\mathbf{p}_0 = \mathbf{e}_z \cdot p_{z,0}$, where $p_{z,0} < 0$, it can be expressed by

$$p_{x,f} = \frac{I_{x,f}}{h_f} = \frac{-r_R\rho_0\Delta}{h_f} \quad \text{with } \Delta \equiv \int_{\phi_0}^{\phi_f} d\phi E_x(\phi) \int_{\phi_0}^{\phi} d\Phi E_x^2(\Phi). \quad (2.41)$$

For the momentum in z-direction one finds

$$p_{z,f} = \frac{p_{z,0}}{h_f} + \frac{h_f^2 - 1 + r_R^2\rho_0^2\Delta^2}{2\rho_0 h_f}. \quad (2.42)$$

An approximate expression for ρ_0 is

$$\rho_0 = n_\mu u_0^\mu = \gamma_0 - p_{x,0} = \sqrt{1 + |\mathbf{p}_0|^2} - p_{x,0} \approx 2 \cdot |\mathbf{p}_0|, \quad (2.43)$$

where $-p_{x,0} = |\mathbf{p}_0| \gg 1$ has been used. Neglecting the $h_f^2 - 1$ term in equation (2.42), because $\rho_0 \gg h_f$, the final deflection angle ζ in x-direction relative to the z-axis is

$$\tan(\zeta) = -\frac{p_{x,f}}{p_{z,f}} \approx \frac{r_R \rho_0 \Delta}{p_{z,0} + r_R^2 \rho_0 \Delta^2 / 2} \approx \frac{-2r_R \Delta}{1 - r_R^2 \Delta^2}, \quad (2.44)$$

for $p_{z,f} < 0$. It can be noticed that the deflection does not depend on the initial momentum, giving this counter-propagating configuration a mirror-like behaviour.

Quasi-monochromatic pulse For a quasi-monochromatic pulse with finite length the x-component of the electric field becomes

$$E_1(\phi) = G(\phi) \xi_1 \sin(\phi + \theta_1) = \sin^2\left(\frac{\phi}{2N}\right) \xi_1 \sin(\phi + \theta_1) \quad (2.45)$$

$$= -\xi_1 \frac{1}{4} \left(e^{\frac{i\phi}{N}} + e^{-\frac{i\phi}{N}} - 2 \right) \frac{1}{2i} \left(e^{i(\phi+\theta_1)} - e^{-i(\phi+\theta_1)} \right), \quad (2.46)$$

with the amplitude ξ_1 , the initial phase θ_1 and the pulse shape envelope defined by $G(\phi) = \sin^2\left(\frac{\phi}{2N}\right)$ in the range $(0, \phi_f)$ and $G(\phi) = 0$ otherwise. N is the number of cycles of the pulse with $N = \phi_f / 2\pi$. Representations of these kinds of pulses can be seen in the figures 2.1a and 2.1c along with their Fourier transforms 2.1b and 2.1d.

The integral Δ_N as defined by equation (2.41) then will be

$$\Delta_N = \int_0^{2\pi N} E_1(\phi) d\phi \int_0^\phi E_1^2(\vartheta) d\vartheta. \quad (2.47)$$

Beginning with the inner integration term one finds that

$$\begin{aligned} E_1^2(\vartheta) &= \xi_1^2 \sin^4\left(\frac{\vartheta}{2N}\right) \sin^2(\vartheta + \theta_1) \\ &= -\frac{\xi_1^2}{64} \left(e^{\frac{2i\vartheta}{N}} + e^{-\frac{2i\vartheta}{N}} + 6 - 4e^{\frac{i\vartheta}{N}} - 4e^{-\frac{i\vartheta}{N}} \right) \cdot \left(e^{2i(\vartheta+\theta_1)} + e^{-2i(\vartheta+\theta_1)} - 2 \right). \end{aligned} \quad (2.48)$$

Integrating the exponential terms in this expression for $E^2(\vartheta)$ adds a multiplication with a constant factor and some additive constants. With equation (5.25 in appendix) many of these terms cancel out after the second integration over full cycles.

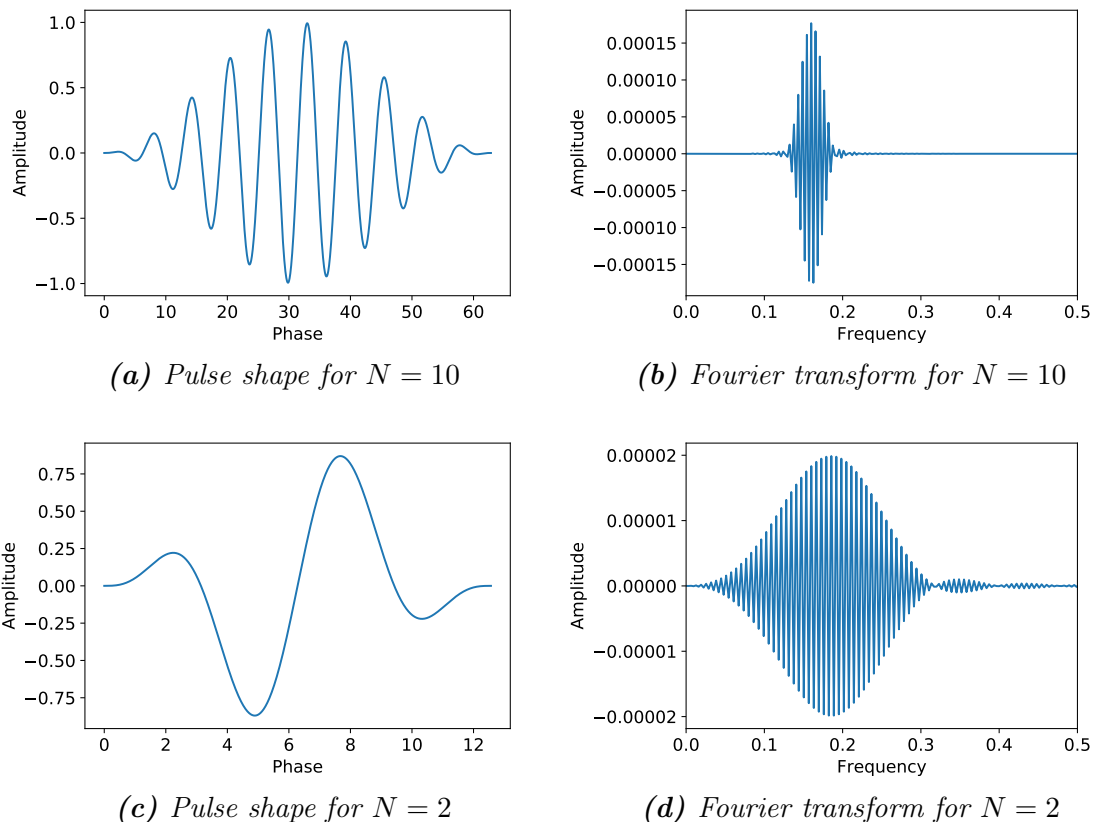


Figure 2.1: Pulse shape and Fourier transform of the finite monochromatic laser field $E_1(\phi)$. The parameters have been set to $\xi_1 = 1$ and $\theta_1 = 0$.

For $N \geq 4$ the resulting integral can be solved by partial integration

$$\Delta_N = \xi_1^3 \int_0^{2\pi N} \sin^2\left(\frac{\phi}{2N}\right) \sin(\phi + \theta_1) d\phi \int_0^\phi \frac{3}{16} d\vartheta \quad (2.49)$$

$$= \frac{3}{16} \xi_1^3 \pi \cos(\theta_1) \frac{N}{N^2 - 1}. \quad (2.50)$$

The transverse momentum gain is shown to be sensitive regarding the laser amplitude and the initial phase but will approach zero for increasing N .

For short pulses of a monochromatic wave, meaning $N = \{2, 3\}$, the integral can be solved exactly and Δ will not vanish. In a few-cycle pulse many frequencies are present, as one can see in the Fourier transform of the pulses, and that the wave is not purely monochromatic (therefore the name *quasi-monochromatic*). For N approaching infinity the Fourier transform sharpens and converges to a Dirac delta distribution. For short N the numerical values of the integral are

$$\Delta_2 = \frac{35}{96} \pi \xi_1^3 \cos(\theta_1), \quad \Delta_3 = \frac{9}{512} \pi \xi_1^3 \cos(\theta_1), \quad (2.51)$$

and therefore the highest deflection can be expected for $N = 2$ cycles.

$N = 1$ is physically meaningless because the pulse would have a non-propagating component. This becomes apparent in the integral over the field:

$$\int_0^{2\pi N} E_1(\phi, N) d\phi = 0, \quad (2.52)$$

which only holds true for $N > 1$.

Two-frequency pulse Now a second harmonic frequency with amplitude ξ_2 and initial phase θ_2 will be added by linear superposition. The field will change to

$$E_2(\phi) = G(\phi) (\xi_1 \sin(\phi + \theta_1) + \xi_2 \sin(2\phi + \theta_2)), \quad (2.53)$$

with the same envelope function as before. Again, the pulse shape can be seen qualitatively for $N = 10$ cycles in figure 2.2a and the Fourier transform in figure 2.2b.

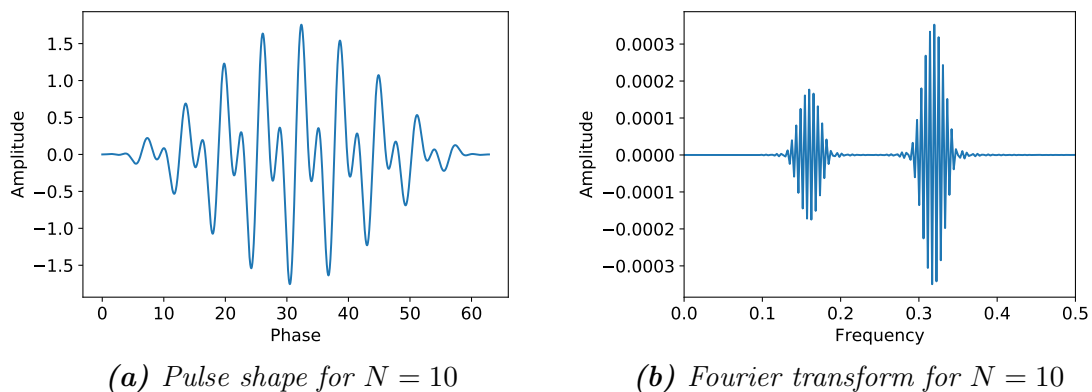


Figure 2.2: Pulse shape and fourier transform of the laser field with second harmonic frequency. The parameters have been set to $\xi_i = 1$ and $\theta_i = 0$.

Expressed as exponential functions, similar to above, the integrand of the inner integral with equation (5.26 in appendix) will become

$$\begin{aligned} E_2^2(\phi) = & -\frac{1}{16} \left(e^{\frac{2i\vartheta}{N}} + e^{\frac{-2i\vartheta}{N}} + 6 - 4e^{\frac{i\vartheta}{N}} - 4e^{\frac{-i\vartheta}{N}} \right) \\ & \cdot \frac{1}{4} \left[\xi_1^2 \left(e^{2i(\vartheta+\theta_1)} + e^{-2i(\vartheta+\theta_1)} - 2 \right) + \xi_2^2 \left(e^{2i(2\vartheta+\theta_2)} + e^{-2i(2\vartheta+\theta_2)} - 2 \right) \right. \\ & \left. + 2\xi_1\xi_2 \left(e^{i(3\vartheta+\theta_1+\theta_2)} + e^{-i(3\vartheta+\theta_1+\theta_2)} - e^{i(\vartheta-\theta_1+\theta_2)} - e^{-i(\vartheta-\theta_1+\theta_2)} \right) \right]. \end{aligned} \quad (2.54)$$

Terms that multiply to constants in E_2^2 will be neglected because they contribute

with a factor of $\frac{1}{N}$ for large N after integration. With equation (5.25 in appendix) the terms that will go to zero can easily be identified.

Therefore, for two frequencies the integral Δ after transforming back to the trigonometric functions reads

$$\begin{aligned} \Delta_N \approx & - \int_0^{2\pi N} \sin^2\left(\frac{\phi}{2N}\right) \left[\xi_1 \sin(\phi + \theta_1) \cdot \int_0^\phi \sin^4\left(\frac{\vartheta}{2N}\right) (-\xi_1 \xi_2 \cos(\vartheta - \theta_1 + \theta_2)) d\vartheta \right. \\ & \left. + \xi_2 \sin(2\phi + \theta_2) \int_0^\phi d\vartheta \sin^4\left(\frac{\vartheta}{2N}\right) \frac{1}{2} (\xi_1^2 \cos(2\vartheta + 2\theta_1)) \right] d\phi. \end{aligned} \quad (2.55)$$

These integrals can be solved analytically with equation (5.27 in appendix) and the following sum for large N remains:

$$\Delta_N \approx \frac{5}{16} \xi_1^2 \xi_2 \pi N \cos(2\theta_1 - \theta_2) - \frac{5}{16} \cdot \frac{1}{4} \xi_1^2 \xi_2 \pi N \cos(2\theta_1 - \theta_2) \quad (2.56)$$

$$\approx \frac{15}{64} N \pi \xi_1^2 \xi_2 \cos(2\theta_1 - \theta_2). \quad (2.57)$$

It can be noticed that the value of Δ_N increases linearly with N while for the one frequency case it averages out for increasing N . It appears to have a resonant initial phase relation as one can see in the cosine term in Δ_N .

Many-frequency pulse For $z \geq 2$ harmonic frequencies the square of the electric field will be

$$E_z^2(\phi) = \sin^4\left(\frac{\phi}{2N}\right) \left[\sum_{i=1}^z \xi_i^2 \sin^2(i\phi + \theta_i) + \sum_{i < j}^{j=z} 2\xi_i \xi_j \sin(i\phi + \theta_i) \sin(j\phi + \theta_j) \right], \quad (2.58)$$

with i, j being positive integer values.

By switching to the exponential form of the sine functions it becomes apparent that the terms that will not become zero or contribute with a factor of $\frac{1}{N}$ after being integrated in Δ can, after changing back to trigonometric functions, be expressed by

$$\begin{aligned} E_z^2(\phi) \approx & \left[- \sum_{i=1}^{i \leq \frac{z}{2}} \frac{1}{2} \xi_i^2 \cos(2(i\phi + \theta_i)) - \sum_{i < j}^{j+i \leq z} \xi_i \xi_j \xi_{j+i} \cos((j+i)\phi + \theta_i + \theta_j) \right. \\ & \left. + \sum_{i < j}^{j=z} \xi_i \xi_j \xi_{j-i} \cos((j-i)\phi + \theta_j - \theta_i) \right] \sin^4\left(\frac{\phi}{2N}\right). \end{aligned} \quad (2.59)$$

With equation (5.27 in appendix) the solution of the entire integral for Δ is easy

to obtain. Further, for $z \geq 3$ there will always be three terms with the same ξ combination and the same constant cosine argument. This leads to the following equation, assuming N to be large:

$$\begin{aligned} \Delta_N \approx & \sum_{i=1}^{i \leq \frac{z}{2}} \xi_i^2 \xi_{2i} N \pi \cos(2\theta_i - \theta_{2i}) \frac{15}{64} \cdot \frac{1}{i} \\ & + \sum_{\substack{j+i \leq z \\ i < j}} \xi_i \xi_j \xi_{j+i} N \pi \cos(\theta_i + \theta_j - \theta_{i+j}) \frac{5}{16} \left(\frac{i^2 + j^2 + ij}{ij(i+j)} \right). \end{aligned} \quad (2.60)$$

The value is linearly increasing with N but has differently weighted terms with different resonance conditions to the initial phase configuration. As both sums in Δ_N are with positive sign, a maximum resonant configuration is given by $\theta_i = 0$. In the following it will be focused on the two frequency case mentioned above, as the qualitative behaviour of the transverse momentum gain is the same as for many harmonic frequencies.

2.5 The numerical integrator

The LL equation (1.9) is a differential equation of second order and therefore it can be solved by numerical integration. For the LL equation without the derivative term and in the unit system introduced above, one finds

$$\frac{du^\mu}{ds} = -F^{\mu\nu} u_\nu - r_R \left(F^{\mu\nu} F_{\alpha\nu} u^\alpha - (F^{\alpha\nu} u_\nu)(F_{\alpha\beta} u^\beta) u^\mu \right). \quad (2.61)$$

With the wavelength of a Ti:sapphire laser $\lambda = 0.8 \mu m$ the numerical value for the constant r_R is approximately

$$r_R = \frac{4\pi e^2}{3mc^2\lambda} \approx 1.47 \cdot 10^{-8}. \quad (2.62)$$

Together with the differential equation for the position

$$\frac{dx^\mu}{ds} = \frac{p^\mu}{m\gamma} \quad \text{with } \gamma = \sqrt{1 + \mathbf{p}^2}, \quad (2.63)$$

the system of equations can be used by a fourth order Runge-Kutta integrator to get numerical results for the momentum and position coordinates. Only the three spatial components (referred to by Latin letters) of equations (2.61) and (2.63) need to be considered. The two sets of equations are coupled; the derivative of the momenta $p_i(t)$ can be calculated by equation (2.61) in the form of $\dot{p}_i = f_i(\mathbf{p}, \mathbf{x}, t)$ but depends

on the position $x_i(t)$ while the derivative of the position coordinates $\dot{x}_i = g_i(\mathbf{p}, t)$ depends on the momenta. The two sets of equations can be written with the help of the 6-dimensional vector \mathbf{a} as follows

$$\mathbf{a}(t) \equiv \begin{pmatrix} \mathbf{p}(t) \\ \mathbf{x}(t) \end{pmatrix} \text{ and therefore } \dot{\mathbf{a}}(t) = \begin{pmatrix} (f_i) \\ (g_i) \end{pmatrix} \equiv \mathbf{B}(\mathbf{a}(t), t). \quad (2.64)$$

With the 7 initial values t_{ini} and $\mathbf{a}(t_{ini})$ the time evolution can be calculated discretely for time steps with size Δt and is approximated by the recursive equation

$$\mathbf{a}(t_0 + \Delta t) = \mathbf{a}_0 + \Delta t \cdot \bar{\mathbf{m}} \equiv \mathbf{a}_0 + \Delta t \cdot \frac{\mathbf{m}_1 + 2\mathbf{m}_2 + 2\mathbf{m}_3 + \mathbf{m}_4}{6}, \quad (2.65)$$

where t_0 denotes the current time step and $\mathbf{a}_0 \equiv \mathbf{a}(t_0)$ the vector at that time step. The values \mathbf{m}_i depend on each other as follows:

$$\mathbf{m}_1 \equiv \mathbf{B}(\mathbf{a}_0, t_0), \quad (2.66)$$

$$\mathbf{m}_2 \equiv \mathbf{B}\left(\mathbf{a}_0 + \frac{\mathbf{m}_1 \Delta t}{2}, t_0 + \frac{\Delta t}{2}\right), \quad (2.67)$$

$$\mathbf{m}_3 \equiv \mathbf{B}\left(\mathbf{a}_0 + \mathbf{m}_2 \frac{\Delta t}{2}, t_0 + \frac{\Delta t}{2}\right), \quad (2.68)$$

$$\mathbf{m}_4 \equiv \mathbf{B}(\mathbf{a}_0 + \mathbf{m}_3 \Delta t, t_0 + \Delta t). \quad (2.69)$$

With the Runge-Kutta integrator the momentum and the position coordinates are calculated simultaneously and are stored at every timestep. The figures that will be shown in the following such as 2.3 and 2.4 can be interpreted as the trajectory that the particle describes in the chosen frame.

This kind of algorithm is more precise than a forward Euler scheme because it averages four slopes of different points near the current time step instead of taking just one. To decrease the runtime of the simulation a balanced time step size Δt needs to be chosen. It has been found that the integrator gives precise results for $\Delta t = 0.03$ (in the unit system introduced above) and this value will be used for all iterations in the following.

2.6 Numerical analysis of a single electron

Infinite laser pulse To investigate the influence of the radiation reaction (RR) force, a purely monochromatic pulse with infinite length is considered. The x-

component of the electric field is chosen as

$$E_{inf}(\phi) = a_0 \cos(\phi), \quad (2.70)$$

where $a_0 \equiv |e| \cdot |\mathbf{E}|/m\omega c$ is the normalised laser amplitude.

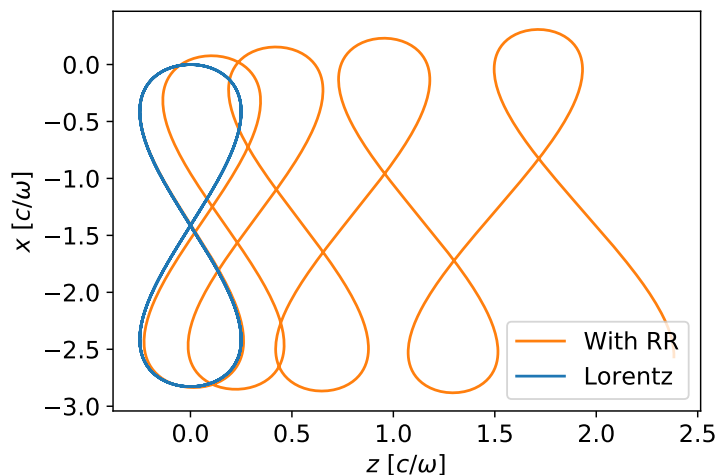


Figure 2.3: Iterated position of an electron in the average rest frame under influence of a purely monochromatic laser field with $a_0 = 100$ and initial electron momentum of $\mathbf{p}_0 = -\mathbf{e}_z \cdot 35.35180406mc$

In figure 2.3 one can see the position of a counter-propagating electron with an initial momentum of $\mathbf{p}_0 \approx -\mathbf{e}_z \cdot 35.4mc$ in z-direction interacting with a monochromatic laser field with $a_0 = 100$. This represents the so called *average rest frame*, meaning the frame where the electron stays in the figure of eight if there was no RR force.

With RR force included, the eight slowly opens and the electron receives acceleration in the direction of the laser pulse propagation. This results in an energy loss and is one reason why the RR force is often referred to as a *damping* or *friction force*.

At this point it may be mentioned that the chosen value for a_0 corresponds to a very high field strength. For a plane wave with linear polarisation the intensity I of the field follows the proportionality $I \propto \mathbf{E}^2$. Therefore with the normalised laser amplitude $a_0 = 100$ and the wavelength of a Ti:sapphire laser $\lambda = 0.8\mu m$ the peak intensity is $I \approx 2.16 \cdot 10^{22} W/cm^2$.

Finite laser pulse Infinite laser pulses are a non physical assumption so to get closer to reality the pulse will be limited to a phase interval (ϕ_0, ϕ_f) with $E_i(\phi) = 0$

outside the interval. For the finite pulse shapes used in section 2.4,

$$E_1(\phi) = \sin^2\left(\frac{\phi}{2N}\right) \xi_1 \sin(\phi + \theta_1) \quad (2.71)$$

$$E_2(\phi) = \sin^2\left(\frac{\phi}{2N}\right) (\xi_1 \sin(\phi + \theta_1) + \xi_2 \sin(2\phi + \theta_2)) \quad (2.72)$$

the evolution of the x, z -position and time-momentum frame give insight into the behaviour of the electron. The result can be seen in the figures 2.4a-2.4d for the one and two frequency pulses.

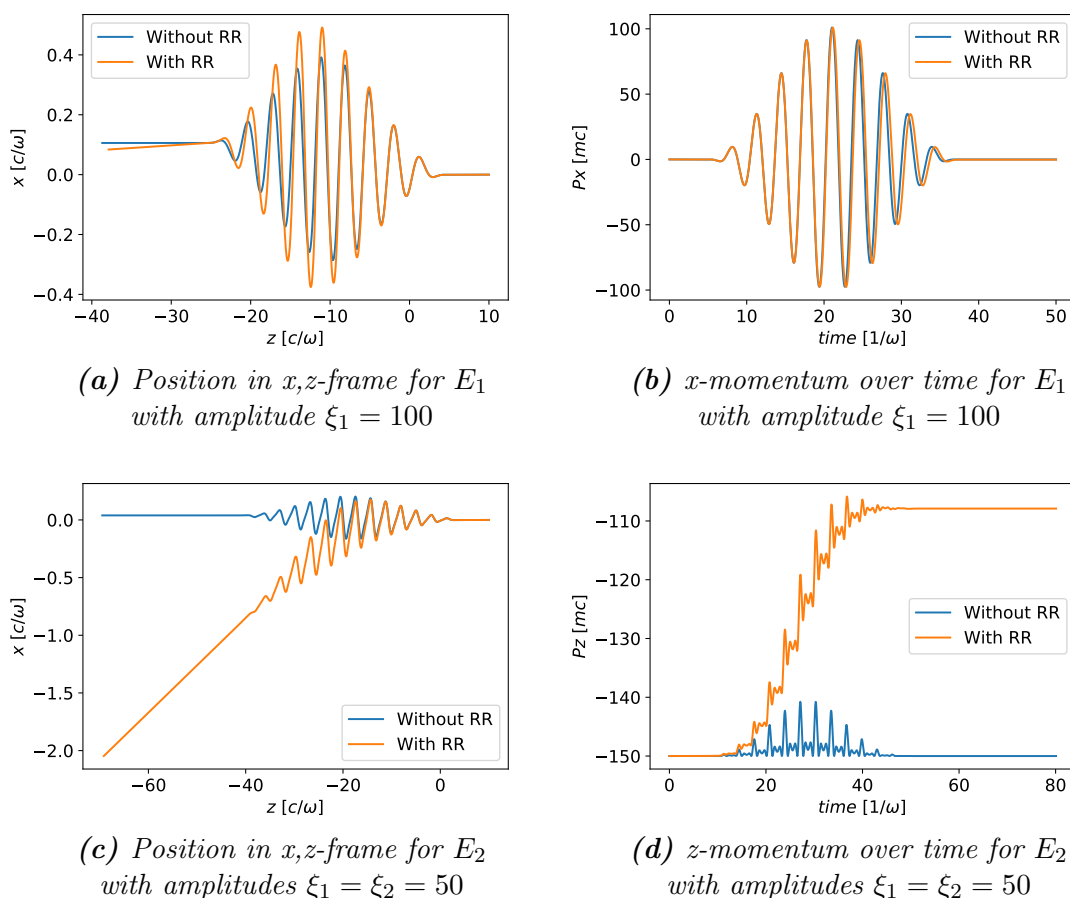


Figure 2.4: Iterated quantities of equations (2.61 and 2.63) by the integrator for the parameters $N = 10$, $\mathbf{p}_0 = -\mathbf{e}_z \cdot 150mc$ and $\theta_i = 0$.

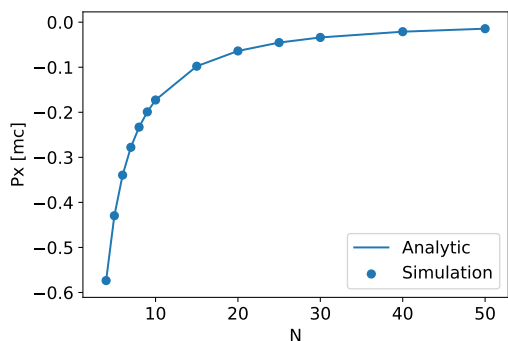
Without the radiation reaction force it becomes clear that in the position frames 2.4a and 2.4c the electron oscillates with the frequency of the electromagnetic field and after the pulse continues to travel in the same direction as before. This is validated by the transverse-momentum gain seen in figure 2.4b; it averages out.

With the RR force the transverse momentum does not average out and the counter-propagating electron gets deflected. As $N = 10$ is a rather long pulse,

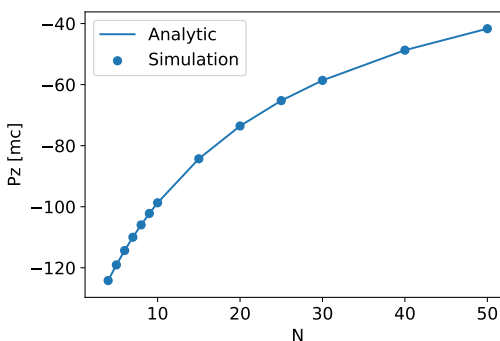
the x-momentum gain is low for the one frequency pulse and barely visible in 2.4a. For the two frequency pulse, in comparison, the direction change is quite large and can be seen in figure 2.4c. In figure 2.4d it can be recognised that with RR force included the electron experiences net acceleration into the propagation direction of the laser pulse.

The y-component of the momentum and the position does not provide interesting information as it stays constant and will therefore be ignored in the following.

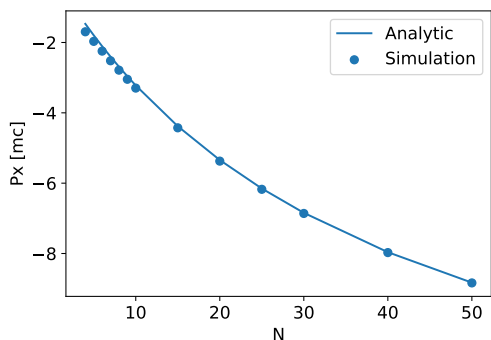
Testing the numerical integrator In order to test the numerical integrator the final value of the momentum components iterated by the simulation are compared to the analytic values that can be calculated with equations (2.41 and 2.42).



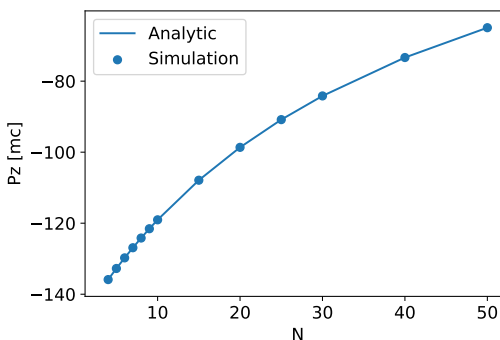
(a) Final x-momentum with pulse E_1 with amplitude $\xi_1 = 100$



(b) Final z-momentum with pulse E_1 with amplitude $\xi_1 = 100$



(c) Final x-momentum with pulse E_2 with amplitudes $\xi_1 = \xi_2 = 50$



(d) Final z-momentum with pulse E_2 with amplitudes $\xi_1 = \xi_2 = 50$

Figure 2.5: Comparison of numeric to analytic value of momentum change for different $N \geq 4$ with an initial momentum of $\mathbf{p}_0 = -\mathbf{e}_z \cdot 150mc$. The upper two figures treat a one frequency pulse where the analytic equation is exact, the lower ones treat the two frequency pulse where the analytic equation is asymptotic.

In the figures 2.5a and 2.5b one can see the result of that comparison for the one frequency laser pulse (2.45). The prediction of the equations (2.41) and (2.42)

match the numerical iterated values exactly.

In figure 2.5c the comparison for the two frequency laser pulse (2.53) shows deviations for small N . This is reasonable because the analytic formula for the momentum gain in the two frequency case (2.57) is an approximate one for large N . In the derivation some additive terms that evolve like $1/N$ have been neglected, resulting in an underestimation of the absolute value by the analytic solution. As can be seen in the figure, for rising N the analytical values become more accurate.

Figure 2.5d shows that the z-momentum does not deviate visibly from the prediction. The term containing Δ in equation (2.42) appears to be so small that it does not matter that Δ is an approximate value, it gets dominated by the other terms, which are exact.

This behaviour has been predicted by the analytic calculations: For a one frequency pulse the transverse momentum gain tends to zero for large N , while for the two frequency pulse it increases with N .

2.7 Simulation of an electron beam

One-frequency pulse A beam of electrons that is counter-propagating to the direction of the laser pulse is being considered. The interaction of the electrons with each other will be neglected.

The initial momentum of the beam follows a Gaussian distribution centering around $\mathbf{p}_0 = -\mathbf{e}_z \cdot 150mc$ with a standard deviation of $\sigma_{P_z} = 10mc$ and $\sigma_{PT} = 1mc$ in the transverse direction. Figure 2.6a shows a representation of this beam in the x,z-momentum frame. The position follows a Gaussian distribution as well but around zero with $\sigma = 0.4\mu m$ in all directions.

Figure 2.6b shows the momentum distribution after a $N = 2$ cycle pulse where the simulation considers only the Lorentz force induced by the laser pulse. As expected no net change in momentum can be seen. The mean momentum in the simulation can be calculated by

$$\bar{\mathbf{p}} = \frac{1}{n} \sum_{k=1}^n (\mathbf{p})_k, \quad (2.73)$$

where n is the number of simulated electrons and $(\mathbf{p})_k$ is the momentum of a single electron k .

In figure 2.6b the final momenta in z- and x-direction are $\bar{p}_z \approx -150mc$ and $\bar{p}_x \approx 0mc$ just as for the initial values where the index f denotes quantities after being hit by the pulse. This has been done for varying numbers of cycles N and initial phase configurations but the resulting plots look the same and the final mean

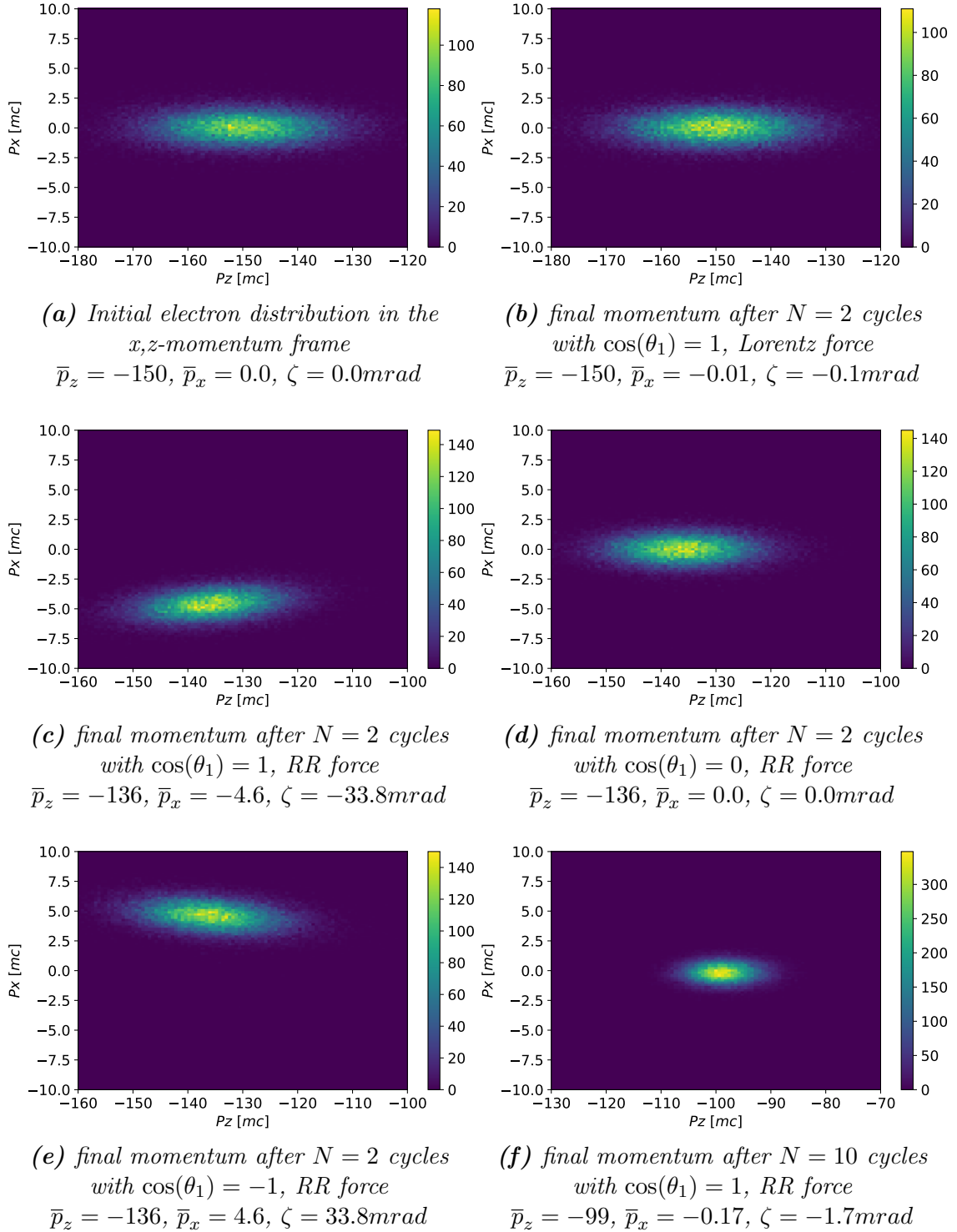


Figure 2.6: Distribution of 50000 simulated electrons in the x,z -momentum frame initially and after being hit by the one-frequency plane-wave laser pulse (2.45) with amplitude $\xi_1 = 100$ (see text for details). The bar on the right-hand side indicates the electron density. The mean momentum values are in units of $[mc]$.

momentum values match the initial ones if solely the Lorentz force is considered.

The figures 2.6c, 2.6d and 2.6e show the beam hit by a laser pulse with $N = 2$ cycles for different initial phases if the RR force is considered in a classical way, according to equation (2.61). A common property is the loss of momentum in z-direction; it stays almost the same for all three of the figures with a mean value of $\bar{p}_z \approx -136mc$. That matches the value from the plane-wave result calculated by equation (2.42) with the corresponding value for Δ of the quasi-monochromatic pulse for a single electron with starting conditions in the center of the distributions. As seen earlier in (2.42) the Δ appears in the analytic equation for the x-momentum but its value appears to be too small to affect the change in z-direction.

In contrary, the x-momentum reacts sensibly to the initial phase. For figure 2.6c one finds agreement for the plane-wave result and simulation mean, both are $\bar{p}_x \approx p_{x,f} \approx -4.6mc$. The same goes for figure 2.6e with a positive sign, respectively, while in figure 2.6d the mean y-momentum is $\bar{p}_x \approx 0mc$, just as for the analytic solution with $p_{x,f} = 0$. It can be seen that by changing the initial phase the whole beam can be deflected into a different direction.

The range of the axes in the figures have the same size, $60mc$ in z-direction and $20mc$ in x-direction, so that another effect can be seen qualitatively: the momentum distribution narrows with higher N in the classical case. It has been shown [17] that under the assumption that $\sigma_{Pz} \ll \bar{p}_z$ where \bar{p}_z is the average momentum in z-direction, the change in standard deviation can be calculated by

$$\sigma_{Pz,f} \approx \frac{\sigma_{Pz,0}}{h_f^2}. \quad (2.74)$$

As derived by Reference [17], this equation is only valid for the classical RR force; if one considers quantum effects the distribution narrows less or broadens.

The standard deviation of momentum in z-direction in the simulation can be calculated with the help of the mean momentum in the following way:

$$\sigma_{Pz,f} = \sqrt{\frac{1}{n} \sum_{k=1}^n [(p_{z,f})_k - \bar{p}_{z,f}]^2}, \quad (2.75)$$

where $(p_{z,f})_k$ is the final momentum in z-direction of a single electron k . Table (2.1) shows the result of the comparison. One can see that the values calculated for the different pulses match the standard deviations obtained by the simulation accurately.

The last thing to mention is that the final momentum distribution underlies a tilt depending on the absolute value of the transverse momentum. As the deflection

Figure	2.6a	2.6b	2.6c	2.6d	2.6e	2.6f
Numeric	10.04	10.16	8.19	8.22	8.19	4.35
Analytic	10.00	-	8.21	8.21	8.21	4.33

Table 2.1: Value of the standard deviation of the momentum in z -direction after the pulse in [mc] for the parameters used in the figures (numeric) compared to the prediction by equation (2.74) (analytic).

angle is expected to be independent of the initial momentum, to be seen in the approximate equation (2.44), it becomes apparent that a low initial momentum results in a low transverse momentum gain and vice versa.

Two-frequency pulse In the following the interaction of the plane-wave laser pulse containing the second harmonic frequency

$$E_2(\phi) = \sin^2\left(\frac{\phi}{2N}\right) (\xi_1 \sin(\phi + \theta_1) + \xi_2 \sin(2\phi + \theta_2)) \quad (2.76)$$

with the electron beam is simulated. The electron beam has the same initial distribution as in section 2.7 so a representation is given in the same figure (2.6a).

The quantum correction is applied according to the semiclassical LL equation (2.27) with the $g(\chi)$ function. One would expect the effect of the corrected RR force to be weaker than in the classical case. In figure 2.7 one can see the simulated momentum distribution after the pulse for two sets of parameters with the classical RR force (2.7a and 2.7c) and with the quantum corrected RR force (2.7b and 2.7d).

Comparing the upper two figures 2.7a and 2.7b qualitatively one finds the deflection to be smaller and the distribution to be broader in the quantum corrected case. Further, the momentum loss in x -direction is smaller as well. The mean values calculated from the simulation can be taken from table 2.2 and they validate this observation.

The same behaviour can be found for the lower two figures 2.7c and 2.7d. Here the initial phase has been chosen so that the deflection will happen in the positive y -direction in order to proof that the general properties stay the same. Again the numerical values can be drawn from table 2.2.

Table 2.2 additionally shows the analytic final values for the same laser pulse for a single electron which is initially at the center of the distributions for position and momentum. As the mean value in the simulation underlies statistical fluctuations the values are expected to not be exactly equal. Compared to the results of the simulation mean value one finds a maximum deviation of $\approx 1.1\%$ to the analytic value.

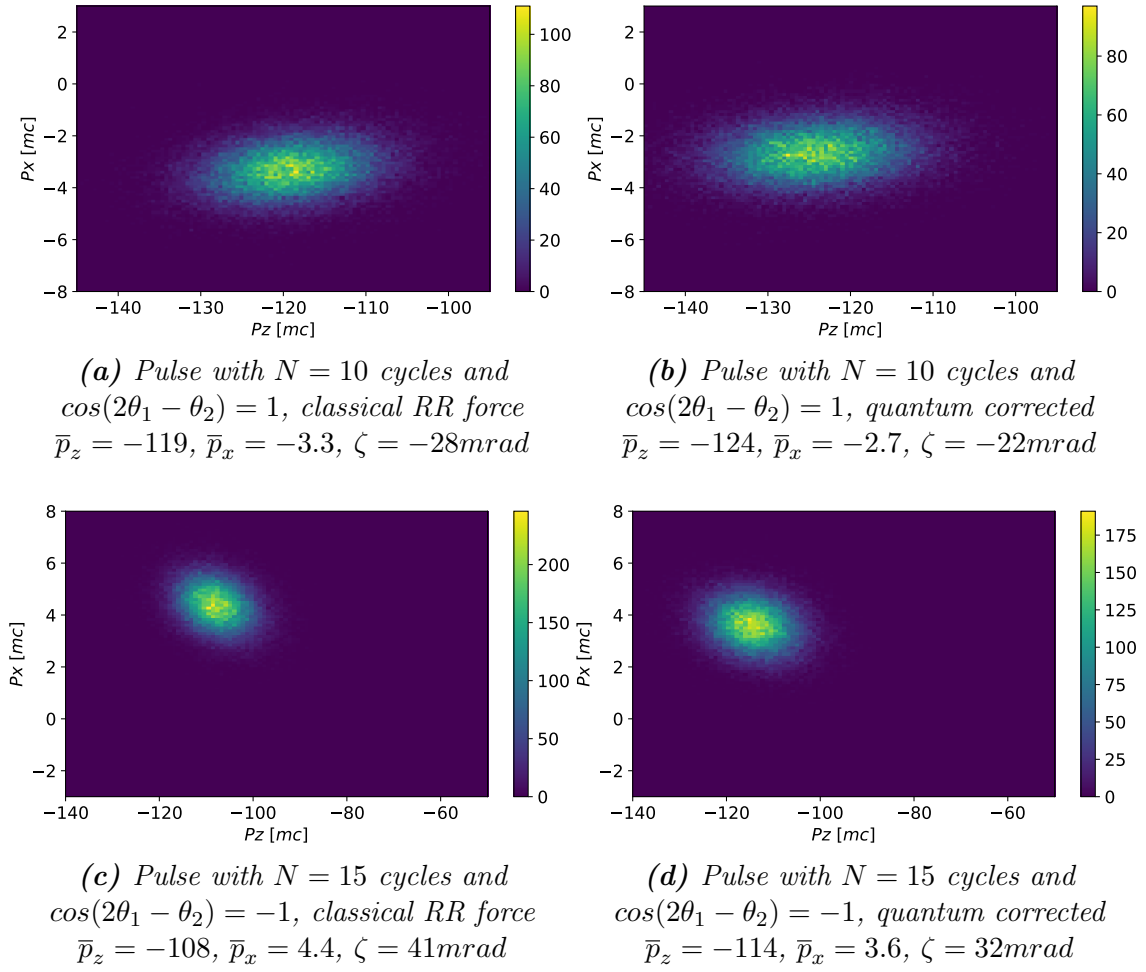
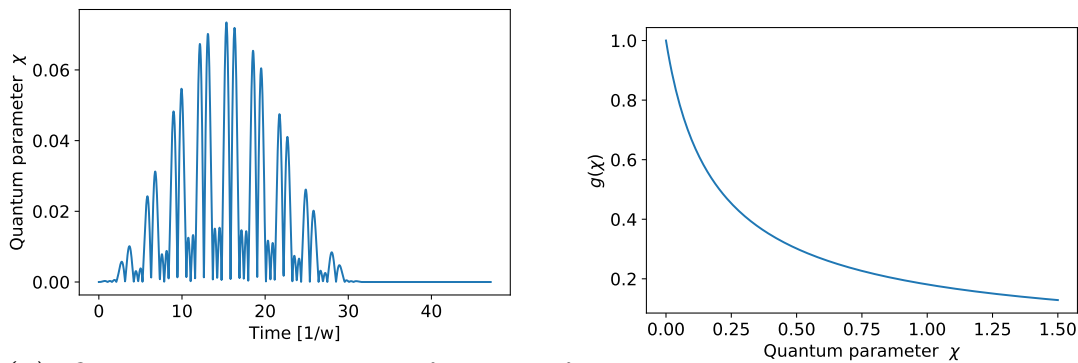


Figure 2.7: Distribution of 50000 simulated electrons in the x,z -momentum frame after being hit by a two-frequency plane-wave laser pulse (2.76) with amplitudes $\xi_i = 50$ with and without the quantum correction. The electrons have the same initial distribution as in the one frequency case above (figure 2.6). The bar on the right-hand side indicates the electron density, the mean momentum is in units of $[mc]$.

Figure	2.7a	2.7b	2.7c	2.7d
Numeric				
\bar{p}_z [mc]	-119.0	-124.2	-107.8	-114.2
\bar{p}_x [mc]	-3.29	-2.66	4.38	3.62
Analytic				
p_z [mc]	-119.0	-124.3	-107.9	-114.2
p_x [mc]	-3.30	-2.66	4.43	3.65

Table 2.2: Values of the final momentum in figures above (2.7). The upper values represent the numerical mean value, the lower ones are the analytic values for a single electron with initial values $\mathbf{p}_0 = -\mathbf{e}_z \cdot 150mc$ and $\mathbf{x}_0 = 0$.

In order to keep track of the magnitude of the quantum parameter χ , its time evolution is drawn in figure 2.8a. As expected, χ vanishes outside of the pulse but has oscillating values during the interaction. For $N = 10$ and $\xi_i = 50$ the maximum value is at ≈ 0.073 which is small enough for assuming that the LL equation is valid. In figure 2.8b one can see that the function $g(\chi)$ decreases steadily for rising χ . The correction function weights the RR term in the LL equation by a factor < 1 in order to account for the overestimated radiation intensity of the classical solution.



(a) Quantum parameter χ as function of time. (b) Correction function g as function of χ .

Figure 2.8: Values of $\chi(\phi)$ and $g(\chi)$ during the two frequency pulse E_2 for $N = 10$ cycles with amplitudes $\xi_i = 50$ and initial phase $\theta_i = 0$.

3 Tightly focused laser pulse

3.1 Field components and geometry

In the facilities where it is possible to reach the extremely high intensities that are necessary to observe the influence of the RR force, the laser pulse shape can be described as *tightly focused*. The model of the pulse that will be used here is taken from Reference [18] and is accurate to the fifth order in the diffraction angle $\epsilon = w_0/z_R$, which is necessary, because small waist radii w_0 are needed. The pulse has a Gaussian transverse profile and a circular cross section along the propagation direction with a waist radius w_0 at the focus $\mathbf{x} = 0$. Figure 3.1 shows the geometry of the laser pulse in the x,z-frame where the positive z-direction was chosen as the propagation direction. with the same normalised unit system as above, the radius

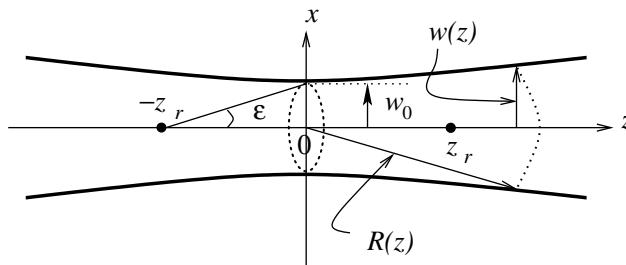


Figure 3.1: Geometry of the laser pulse. The figure is taken from Reference [18] but some parts have been erased.

of the cross section at any point on the z-axis is

$$w(z) = w_0 \sqrt{1 + \left(\frac{z}{z_R}\right)^2}, \quad (3.1)$$

where $z_R \equiv w_0^2/2$ is the Rayleigh length. With *radius* the point is meant where the intensity has decreased to $1/e^2$ of its maximum value. With linear polarisation in

x-direction the electric field components are given by

$$E_x = E \left[S_0 + \epsilon^2 \left(\xi^2 S_2 - \frac{\rho^4 S_3}{4} \right) + \epsilon^4 \left(\frac{S_2}{8} - \frac{\rho^2 S_3}{4} - \frac{\rho^2(\rho^2 - 16\xi^2)S_4}{16} - \frac{\rho^4(\rho^2 + 2\xi^2)S_5}{8} + \frac{\rho^8 S_6}{32} \right) \right], \quad (3.2)$$

$$E_y = E \xi v \left[\epsilon^2 S_2 + \epsilon^4 \left(\rho^2 S_4 - \frac{\rho^4 S_5}{4} \right) \right], \quad (3.3)$$

$$E_z = E \xi \left[\epsilon C_0 + \epsilon^3 \left(-\frac{C_2}{2} + \rho^2 C_3 - \frac{\rho^4 C_4}{4} \right) + \epsilon^5 \left(-\frac{3C_3}{8} - \frac{3\rho^2 C_4}{8} - \frac{17\rho^4 C_5}{16} - \frac{3\rho^6 C_6}{8} + \frac{\rho^8 C_7}{32} \right) \right], \quad (3.4)$$

while the magnetic field components are

$$B_x = 0, \quad (3.5)$$

$$B_y = E \left[S_0 + \epsilon^2 \left(\frac{\rho^2 S_2}{2} - \frac{\rho^4 S_3}{4} \right) + \epsilon^4 \left(-\frac{S_2}{8} + \frac{\rho^2 S_3}{4} + \frac{5\rho^2 S_4}{16} - \frac{\rho^6 S_5}{4} + \frac{\rho^8 S_6}{32} \right) \right], \quad (3.6)$$

$$B_z = E v \left[\epsilon C_1 + \epsilon^3 \left(\frac{C_2}{2} + \frac{\rho^2 C_3}{2} - \frac{\rho^4 C_4}{4} \right) + \epsilon^5 \left(\frac{3C_3}{8} + \frac{3\rho^2 C_4}{8} + \frac{3\rho^4 C_5}{16} - \frac{\rho^6 C_6}{4} + \frac{\rho^8 C_7}{32} \right) \right]. \quad (3.7)$$

Here $\xi \equiv x/w_0$, $v \equiv y/w_0$ and the diffraction angle is defined as $\epsilon \equiv w_0/z_R$. The amplitude function E describes the transverse decrease with a Gaussian function

$$E = E_0 \frac{w_0}{w} \exp \left(-\frac{r^2}{w^2} \right) \cdot G(\phi_p), \quad (3.8)$$

with $r^2 \equiv x^2 + y^2 \equiv \rho^2 w_0^2$, the laser amplitude E_0 and where $G(\phi_p)$ is the temporal envelope function. The two functions in the field components are

$$S_n \equiv \left(\frac{w_0}{w} \right)^n \sin(\phi + n\phi_G), \quad (3.9)$$

$$C_n \equiv \left(\frac{w_0}{w} \right)^n \cos(\phi + n\phi_G), \quad (3.10)$$

for integer values of n . The phase ϕ splits into 4 summands where every term is defined as it appears in the following sequence

$$\phi \equiv \phi_0 + \phi_p - \phi_R + \phi_G \equiv \phi_0 + (t - z) - \frac{r^2}{2R} + \arctan\left(\frac{z}{z_R}\right), \quad (3.11)$$

Here ϕ_0 is a constant initial phase and the curvature radius is $R(z) \equiv z + z_R^2/z$.

3.2 Head-on collision

Two-frequency pulse The laser pulse will contain two frequencies with wavelengths $\lambda_1 = 0.8\mu m$ and $\lambda_2 = 0.4\mu m$ which can mathematically be realised by linear superposition. The two frequency components have normalised laser amplitudes of $E_{0,1} = 40$ and $E_{0,2} = 28$ and the initial phases $\phi_{0,1} = 0$ and $\phi_{0,2} = \{0, \dots, 2\pi\}$. The waist radius at the focus is $w_0 = 5\mu m$.

The laser pulse will have a temporal envelope following a hyperbolic secant function

$$G(\phi_p) = \text{sec}(\varphi) = \frac{2}{e^\varphi + e^{-\varphi}}, \quad \text{with } \varphi \equiv \frac{2\phi_p}{\tau_0} \cdot \text{arccosh}\sqrt{2}. \quad (3.12)$$

with the full width at the half maximum (FWHM) τ_0 of the intensity, chosen to be $\tau_0 = 70fs \approx 26cycles$ for this simulation. This satisfies the condition that

$$\frac{dG(\phi_p)}{d\phi_p} \ll G(\phi_p), \quad (3.13)$$

which is necessary for the field model to be valid, as pointed out by Reference [19].

The electron beam will have an initial momentum in the negative z-direction which follows a Gaussian distribution centering at $\mathbf{p}_0 = -\mathbf{e}_z \cdot 165mc$ with a spread of $\sigma_{P_z} = 12mc$ and $\sigma_{PT} = 1mc$ in transverse direction. Further, the position follows a Gaussian distribution with a spread in z-direction of $\sigma_z = 0.5\mu m$ and in transverse direction $\sigma_T = 0.25\mu m$.

In the figures 3.2a and 3.2b one can see the x- and z-momentum distribution after the pulse for different initial phases when only the Lorentz force is considered. Similar to the plane-wave case the electrons are not able to gain momentum in any direction and the change in initial phase has no effect.

When considering the RR force, as shown in figures 3.2c and 3.2d, the electrons lose a large part of their initial z-momentum, but the same amount for both initial phases with $\bar{p}_z \approx 81mc$. For comparison the plane wave predicts the final z-momentum to be at $p_{z,f} \approx -79mc$. The x-momentum gain appears to be sensitive to the phase configuration with $\bar{p}_x \approx -6.9mc$ for figure 3.2c and $\bar{p}_x \approx 0.1mc$ for

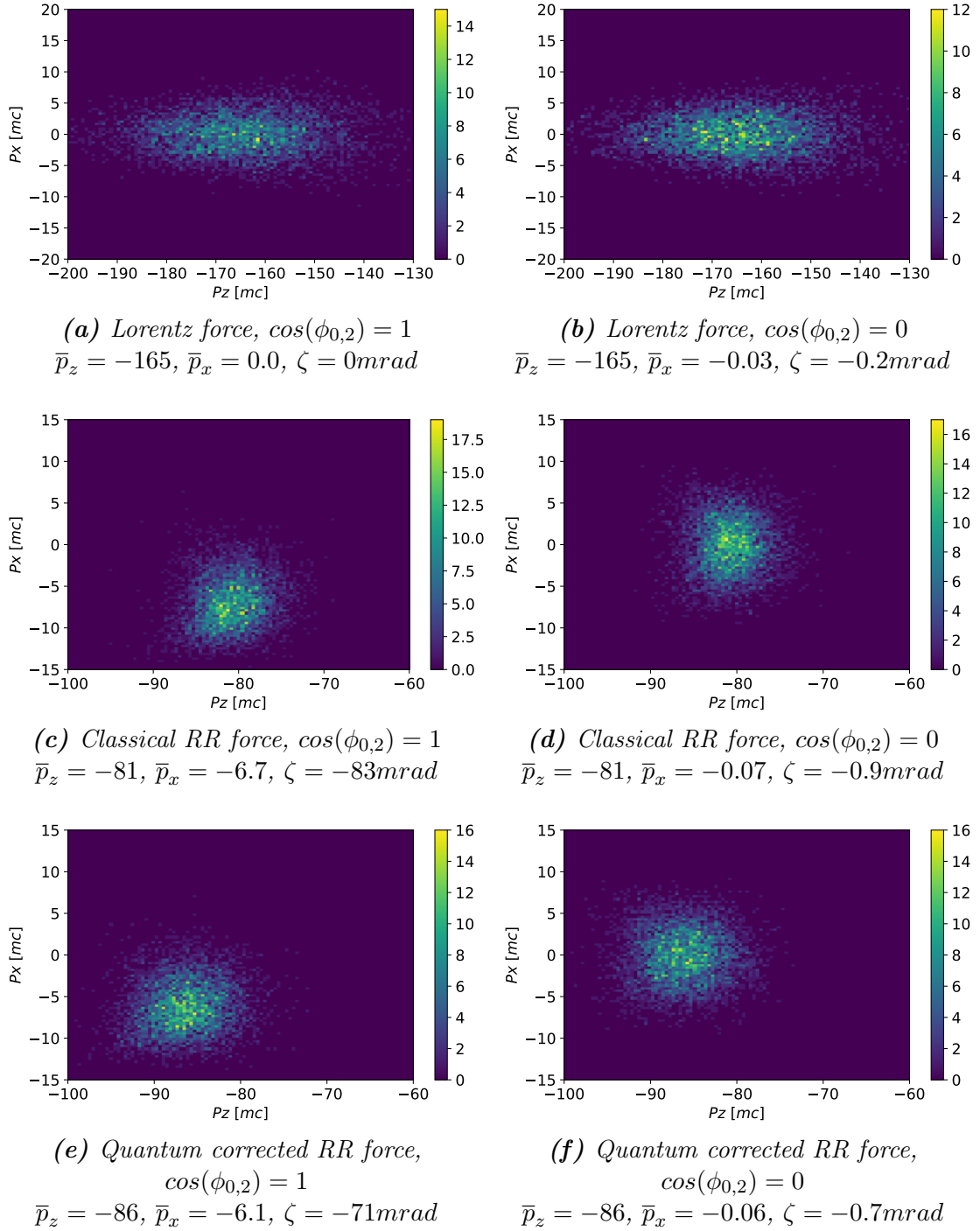


Figure 3.2: Momentum of 5000 electrons in the x,z -frame after the head-on collision with a tightly focused laser pulse containing two frequencies (details in text). The bar on the right-hand side indicates the electron density. The mean momentum is in units of $[mc]$.

figure 3.2d in qualitative agreement to the plane wave values with $p_{x,f} \approx -5.8mc$ for figure 3.2c and $p_{x,f} \approx 0mc$ for figure 3.2d, respectively.

The influence of the quantum correction from section 2.2 applied to the LL equation that calculates the position and momentum coordinates also is in accordance with the plane-wave result; the effect of the RR force becomes weaker with the quantum correction. The z-momentum in the figures 3.2e and 3.2f is $\bar{p}_z \approx -86mc$ while for the plane wave it is $p_{z,f} \approx -85mc$. Furthermore, the transverse momentum becomes $\bar{p}_x \approx -6.1mc$ in figure 3.2e and $\bar{p}_x \approx -0.1mc$ in figure 3.2f. This is in agreement with the plane-wave values of $p_{x,f} \approx -5.3mc$ and $p_{x,f} \approx 0mc$.

One-frequency pulse In order to see the effect of the radiation reaction force in the quasi-monochromatic case, the pulse needs to be short. The temporal envelope function $G(\phi_p)$ follows a Gaussian function with

$$G(\phi_p) = \exp\left(-\frac{\phi_p^2}{\tau_0^2} \cdot 2 \ln(2)\right), \quad (3.14)$$

where τ_0 determines the FWHM of the intensity. Here, condition 3.13 is violated in the case of $|\phi_p| \gg \tau_0$ according to Reference [19], but for small ϕ_p the model is expected to describe the fields well. In contrast to the \sin^2 envelope used in the analytic solution, the Gaussian envelope cannot be set to an exact number of cycles. For one frequency the highest deflection is expected at $N = 2$ cycles, so the value of the FWHM is chosen to be $\tau_0 = \lambda = 0.8\mu m$. In order to keep the pulse shape anti-symmetric in the center, the only initial phases used are $\phi_0 = \{0, \pi\}$, inducing a sine function in equation (3.9).

In the simulations the initial energy of the electrons follows a Gaussian distribution centering around $W = \gamma mc = 200mc$ with a spread of 0.1% in the transverse direction and an angular aperture of 0.01 *mrad*. The Gaussian position distribution has a transverse spread of $\sigma_T = 1\mu m$ and a length of $\sigma_z = 0.1\mu m$ while the waist radius of the beam is $w_0 = 10\mu m$.

In the plots in the left column of figure 3.3 the momentum after the interaction of the beam with a laser pulse with $E_0 = 70$ can be seen for the three different forces: the Lorentz force, the classical RR force and the quantum corrected RR force. With the Lorentz force (3.3a) the beam expands in the momentum frame but does not change its central position. In the RR force case (3.3c) the electrons hit in the center of the pulse experience the most energy loss and the distribution forms a half-moon shape at a lower mean momentum. Integrating the Δ -integral (2.41) numerically and using equation 2.44, the expected deflection is $\approx 3.5\text{mrad}$ and matches the

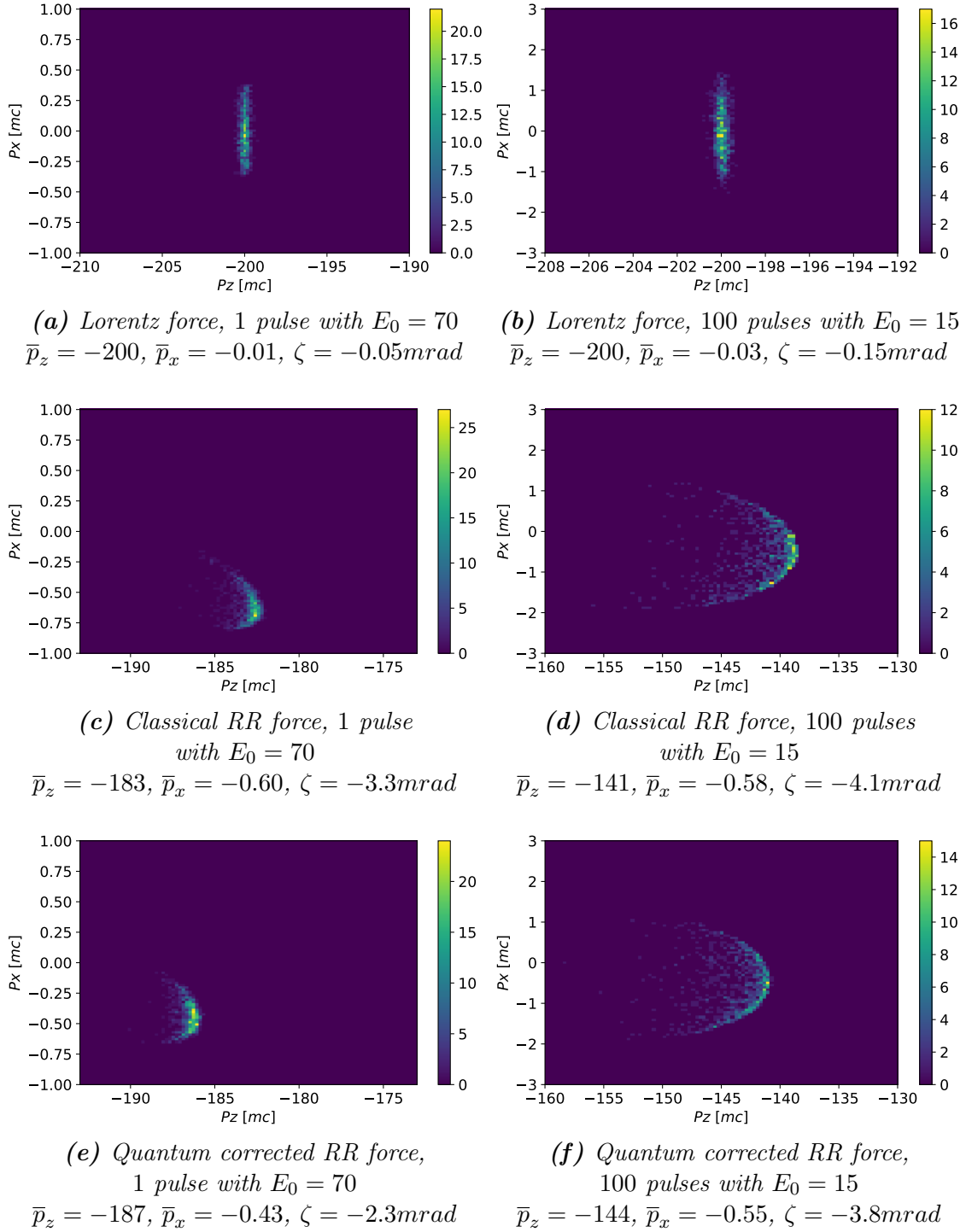


Figure 3.3: Momentum of 1000 electrons in the x,z -frame after the head-on collision with a quasi-monochromatic tightly focused laser pulse for one pulse and for a train of 100 pulses (see text for details). The bar on the right-hand side indicates the electron density.

deflection calculated from the mean in figure 3.3c with $\approx -3.3mrad$. The quantum correction weakens the effect of the RR force and a deflection of $\approx -2.3mrad$ is found in figure 3.3e along with more final energy compared to the classical RR force.

As high intensity pulses with a large waist radius are hard to achieve, the interaction of a less intense train of 100 pulses is simulated, to be seen in the right column of figure 3.3. It is assumed that the electrons hit all pulses at their focus. The total interaction length in the simulation is $0.50mm$ which is similar to $2z_R \approx 0.79mm$. The Rayleigh length gives a scale for the decreasing intensity in the z-direction, so the assumption can be made but the result has to be taken with care. The simulation could be made more realistic with a focus that increases with the number of pulses. Comparing figure 3.3d to the single pulse interaction in figure 3.3c, the spread in the momentum is larger due to the longer interaction time, even for the Lorentz force (3.3b). With classical RR force, the deflection according to the Δ -integral is $3.4mrad$ and in figure 3.3d it is at $\approx -4.1mrad$ while in the quantum corrected RR force it is $\approx -3.8mrad$. The spread is large so the mean value is not that informative and probably a reason why the deflection deviates from the expectation. Another reason could be, that the electron beam hits the incoming pulses eccentrically after some interactions and the final deflection is changed by that. The effect of the quantum correction in figure 3.3f is less than for the single pulse case, because its strength depends mainly on the momentum and the field amplitude, the latter being smaller for the train of pulses.

3.3 Oblique incidence collision

As seen in the plane wave result for a quasi-monochromatic pulse, the momentum gain of the electrons in the direction transverse to the initial propagation direction decreases with rising pulse length. In order to make the pulse extremely short for the electron beam, the beam can enter the focus in a right angle to the laser propagation direction.

The same model for the tightly focused laser pulse from Reference [18] is used. The waist radius w_0 determines the transverse profile of the pulse and therefore the length of the laser pulse experienced by the electron. The temporal envelope can be considered long and can for simplicity be set to $G(\phi_p) = 1$, thus satisfying condition 3.13. The laser pulse has a wavelength of $\lambda = 0.8\mu m$ and a normalised laser amplitude of $E_0 = 100$.

In the simulation for figures 3.4, 3.5 and 3.6 the electrons are entering the focus

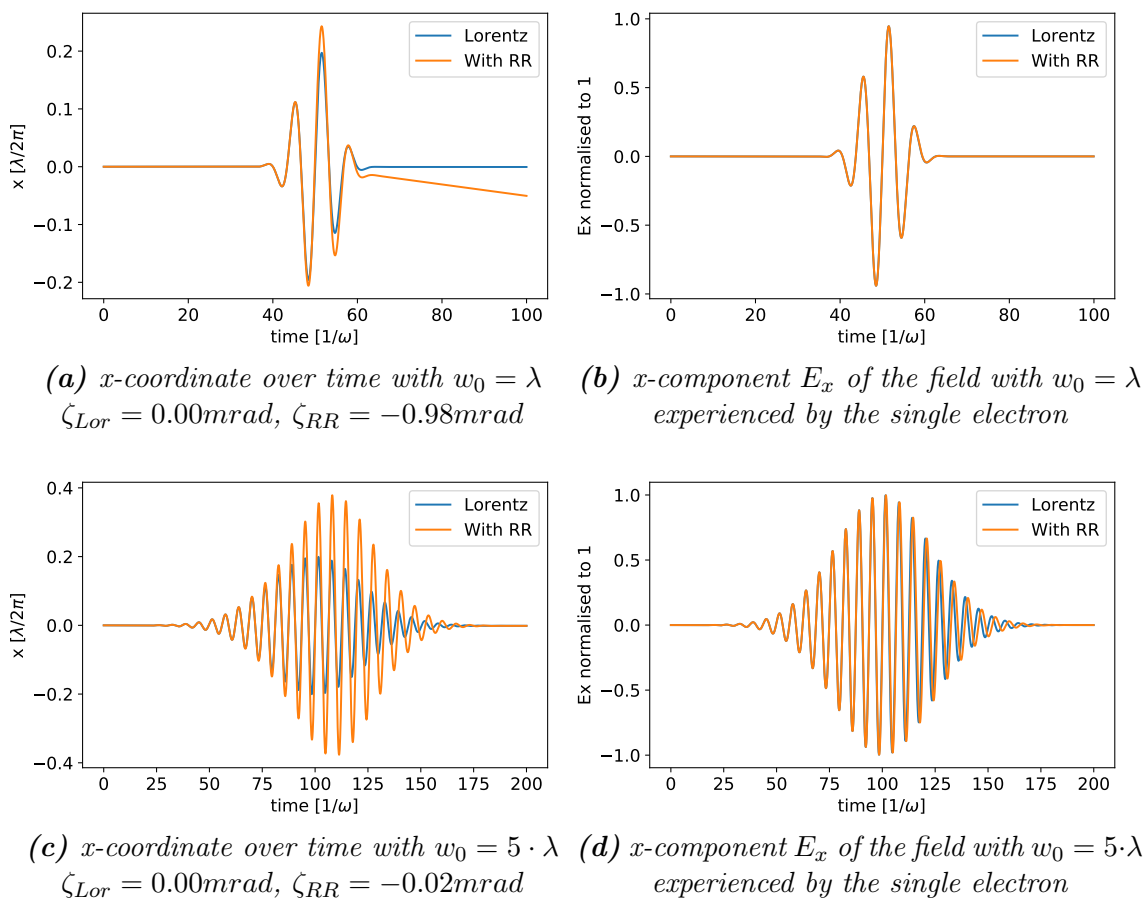


Figure 3.4: Interaction of a single electron with initial conditions $\mathbf{p}_0 = -\mathbf{e}_y \cdot 500mc$ and $\mathbf{x}_0 = \mathbf{e}_y \cdot 100\lambda/2\pi$ with a tightly focused laser pulse in the oblique incidence case. The laser pulse has the amplitude $E_0 = 100$ and no temporal envelope.

from the positive y -direction with a kinetic energy of $\gamma mc = 500mc$ with a spread in y -direction of $\sigma_{Py} = 0.1\%$ and an angular aperture of 0.01 mrad . Because of the small waist radius, the spatial shape of the electron beam needs to be narrow in transverse direction but can be long in y -direction. It follows a Gaussian distribution with $\sigma_T = 0.1\mu m$ in transverse direction and a length of $\sigma_y = 1\mu m$ in y -direction.

In figures 3.4b and 3.4d the x -component of the electric field experienced by a single electron that is initially travelling along the negative y -axis with $x = z = 0$ is shown. In figure 3.4b for $w_0 = \lambda$ only a few-cycle pulse can be seen and deflection in x -direction can be expected according to the head-on plane wave solution with RR force. In figure 3.4d the effective pulse has many cycles, corresponding to a low deflection for the head-on plane wave solution. This is validated in figures 3.4a and 3.4c where the Lorentz force does not induce deflection in x -direction, while the RR force does.

The figures 3.5 and 3.6 show the influence of the RR effect for many electrons for

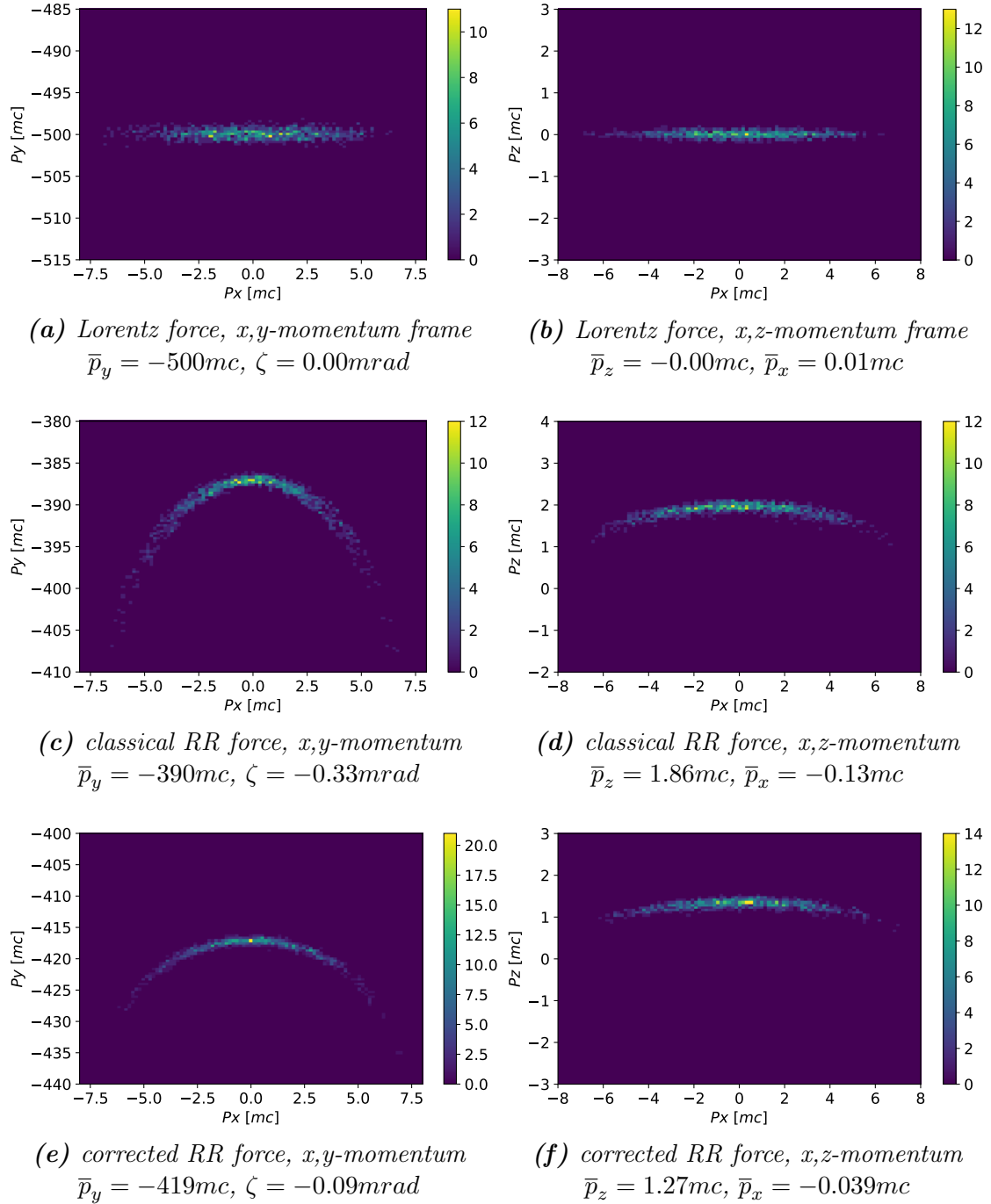


Figure 3.5: Final momentum after the interaction of 1000 electrons with a tightly focused laser pulse in the oblique incidence case. The laser pulse has a waist radius of $w_0 = \lambda$, the amplitude $E_0 = 100$ and no temporal envelope. The bar on the right-hand side indicates the electron density.

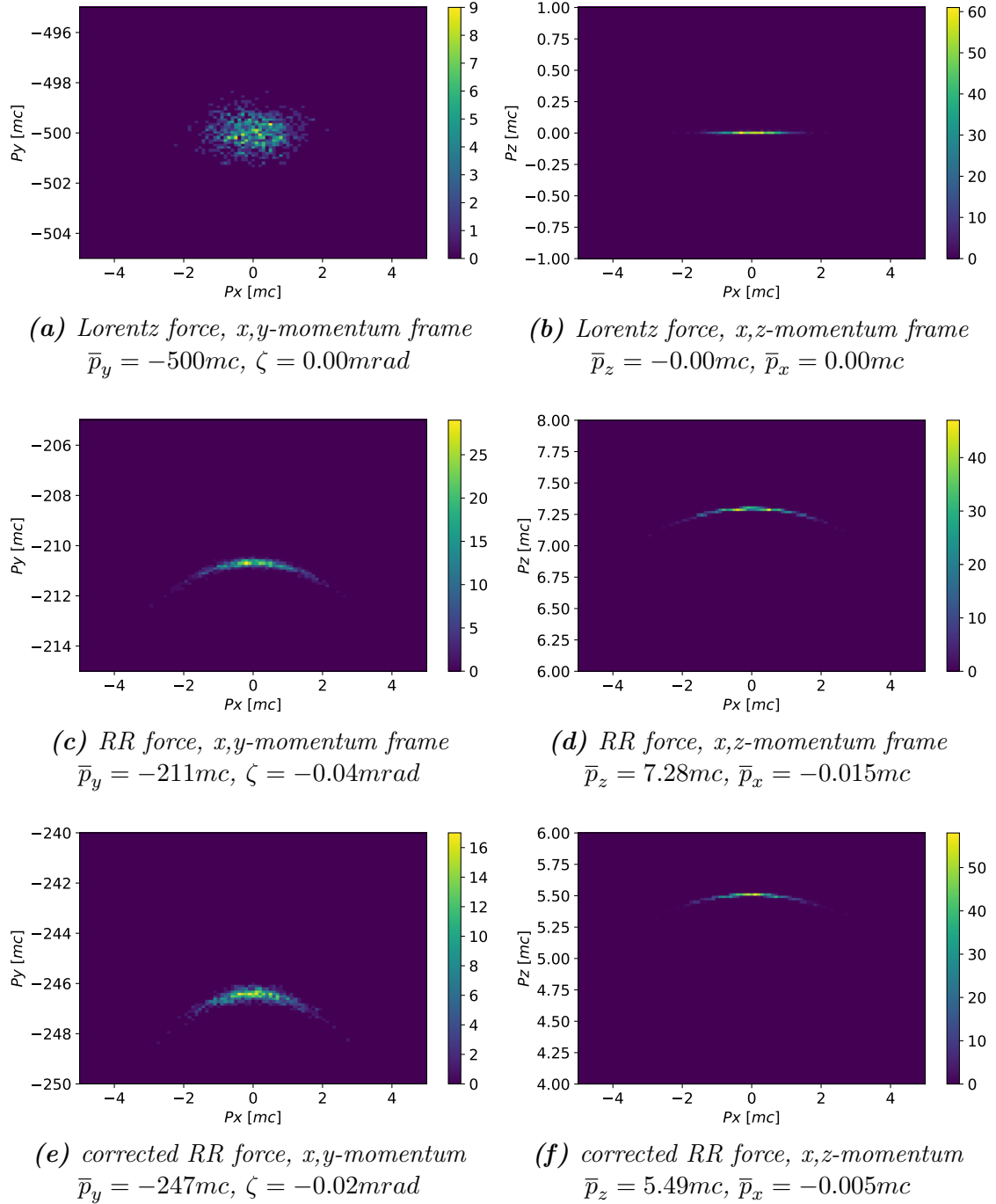


Figure 3.6: Final momentum after the interaction of 1000 electrons with a tightly focused laser pulse in the oblique incidence case. The laser pulse has a waist radius of $w_0 = 5 \cdot \lambda$, the amplitude $E_0 = 100$ and no temporal envelope. The bar on the right-hand side indicates the electron density.

a waist radius of $w_0 = \lambda$ and $w_0 = 5\lambda$, respectively. The Lorentz force in figures 3.5a, 3.5b and 3.6a, 3.6b does not alter the mean momentum after the interaction with the laser pulse for both waist radii.

With RR included the electrons experience deflection in x-direction. This can be seen in the momentum in the figures 3.5c and 3.5d for a pulse with waist radius $w_0 = \lambda$. The mean deflection angle in x-direction with respect to the y-axis is $\zeta = -0.33\text{mrad}$, which is small compared to the values in the head-on interactions. As the intensity of the field decreases for electrons with $|z| > 0$, the overestimated deflection by the single electron in figure 3.4a with $\zeta_{RR} = -0.98\text{mrad}$ is reasonable. This is also the reason for the parabolic shape of the distributions: The strength of the RR effect increases with the intensity and is stronger for electrons that hit the pulse closer to the center of the focus.

In the case where $w_0 = 5\lambda$ the x-momentum in figures 3.6c and 3.6d leads to a deflection of $\zeta = -0.04\text{mrad}$ when considering the RR force. This follows the expectation, as the deflection for the single electron in figure 3.6e is $\zeta_{RR} = -0.02\text{mrad}$ and is also in accordance with the qualitative prediction that only a short one-frequency pulse shows noticeable deflection in x-direction.

Besides the deflection in x-direction with the RR force, the electrons lose a significant amount of their initial momentum (see figures 3.5c and 3.6c) and are accelerated into the direction of laser propagation (see figures 3.5d and 3.6d). Both of these effects are stronger for the field with larger waist radius, because the interaction time is longer.

All three effects are reduced when the quantum correction is applied. This is shown in figures 3.5e and 3.5f for $w_0 = \lambda$ where the deflection in x-direction decreases to $\zeta = -0.09\text{mrad}$, the final absolute value of the y-momentum is higher with $\bar{p}_y = -419mc$ and the momentum gain in z-direction is smaller with $\bar{p}_z = 1.27mc$. In the case where $w_0 = 5 \cdot \lambda$ in figures 3.6e and 3.6f the deflection decreases to $\zeta = -0.02\text{mrad}$, less y-momentum is lost with $\bar{p}_y = -247mc$ and the momentum in propagation direction of the laser pulse is smaller with $\bar{p}_z = 5.49mc$.

Summarising it can be stated out that the deflection behaviour in x-direction is qualitatively the same as in the head-on collision and the RR typical effects, such as loss of energy and acceleration into z-direction, appear as well.

4 Conclusion

In this thesis the interaction of relativistic electrons with superstrong laser pulses under the effect of the radiation reaction (RR) force from classical electrodynamics is studied in a theoretical way by numerical integration. At first, given a differential equation for the position and momentum of the electron, an exact solution is derived analytically for the case of a plane-wave pulse. The solution obtained is used to validate the proper functionality of the numerical integrator and agreement is found by comparison of the iterated quantities. While the Lorentz force is not able to change the momentum of the electron after closed cycles of the plane-wave pulse, the RR force accelerates the charge into the laser pulse propagation direction and can induce a transverse momentum, mainly depending on the initial phase and the field amplitude. The simulation of a beam of electrons shows to follow the expectation that the deflection behaviour of the beam caused by a head-on collision with the laser pulse can be controlled by changing the initial phase configuration and that the deflection angle is independent of the initial electron momentum. The head-on collision with a tightly focused laser pulse with two frequencies does not differ significantly from the plane wave case. The one-frequency head-on interaction also shows to follow the expectation of the plane wave but the momentum distribution changes shape because of the focused structure. A train of quasi-monochromatic pulses with less intensity appears to be an alternative way to see the effect of the RR force experimentally, as lower intensities are easier to achieve. Furthermore it is found that when injecting electrons into the focus of the tightly focused laser pulse at a right angle to the propagation direction, the same RR effects can be observed as in the head-on collision. The quantum correction is applied to account for the overestimation of the emitted radiation by the electron considering that the electron can not produce photons exceeding its own kinetic energy. This results in the effect of the RR force to be weaker than in the classical case, meaning that the deflection angle and the momentum loss in propagation direction is smaller. Since the emission of radiation is a stochastic effect, the resulting altered spectrum could be taken into account to make the simulation more realistic.

5 Mathematical appendix

5.1 Picard iteration for the classical solution

Theorem of Picard [20]:

For a given differential function $d\tilde{u}^\mu/d\phi = f^\mu(\phi, \tilde{u}^\alpha(\phi))$ and a starting value $\tilde{u}^\mu(\phi_0) = h(\phi_0)u^\mu(\phi_0) = u_0^\mu$, the solution can be approximated by

$$\gamma^{[k+1]\mu}(\phi) = \gamma^{[0]\mu} + \int_{\phi_0}^{\phi} f^\mu(\Phi, \gamma^{[k]\alpha}(\Phi)) d\Phi \quad \text{with } \gamma^{[0]\mu} = \tilde{u}_0^\mu, \quad (5.1)$$

and converges to the solution for increasing k. Applying this formalism to the new LL equation (2.18) yields for $k = 1$

$$\begin{aligned} \gamma^{[1]\mu}(\phi) &= \tilde{u}_0^\mu - \int_{\phi_0}^{\phi} \frac{\gamma^{[0]\alpha} \eta_{\alpha\nu}}{m\rho_0} \left(h(\Phi) e F^{\mu\nu}(\Phi) + \frac{2}{3} \alpha \frac{e}{m} F'^{\mu\nu}(\Phi) \rho_0 \right) d\Phi \\ &\quad + \int_{\phi_0}^{\phi} n^\mu \frac{2}{3} \frac{\alpha}{m} h(\Phi) (\xi_1^2(\Psi'_1(\Phi))^2 + \xi_2^2(\Psi'_2(\Phi))^2) d\Phi \end{aligned} \quad (5.2)$$

$$\begin{aligned} &= \tilde{u}_0^\mu - \int_{\phi_0}^{\phi} \frac{\tilde{u}_{0,\nu}}{\rho_0 m} \left(h(\Phi) e (f_1^{\mu\nu} \Psi'_1(\Phi) + f_2^{\mu\nu} \Psi'_2(\Phi)) \right. \\ &\quad \left. + \frac{2}{3} \alpha \frac{e}{m} \rho_0 (f_1^{\mu\nu} \Psi''_1(\Phi) + f_2^{\mu\nu} \Psi''_2(\Phi)) \right) d\Phi + \int_{\phi_0}^{\phi} \frac{n^\mu}{\rho_0} h(\Phi) h'(\Phi) d\Phi \end{aligned} \quad (5.3)$$

$$= \tilde{u}_0^\mu - \frac{1}{\rho_0} \frac{e}{m} (f_1^{\mu\nu} I_1(\phi) + f_2^{\mu\nu} I_2(\phi)) \tilde{u}_{0,\nu} + \frac{1}{2\rho_0} (h^2(\phi) - 1) n^\mu, \quad (5.4)$$

where $I_j(\phi)$ is defined as

$$I_j(\phi) \equiv \int_{\phi_0}^{\phi} \left(h(\Phi) \Psi'_j(\Phi) + \frac{2}{3} \alpha \frac{\rho_0}{m} \Psi''_j(\Phi) \right) d\Phi, \quad (5.5)$$

and the identity for the following integral that can be acquired by partial integration and the relation $h(\phi_0) = 1$

$$\int_{\phi_0}^{\phi} h h' d\Phi = - \int_{\phi_0}^{\phi} h h' d\Phi + h^2(\phi) - h^2(\phi_0) = \frac{1}{2} (h^2(\phi) - 1). \quad (5.6)$$

For the next step $k = 2$ one finds

$$\begin{aligned} \gamma^{[2]\mu}(\phi) &= \tilde{u}_0^\mu - \int_{\phi_0}^{\phi} \frac{1}{\rho_0 m} \left(h(\Phi) e F^{\mu\nu}(\Phi) + \frac{2}{3} \alpha \frac{e}{m} F'^{\mu\nu}(\Phi) \rho_0 \right) \eta_{\alpha\nu} \gamma^{[1]\alpha}(\Phi) d\Phi \\ &\quad + \int_{\phi_0}^{\phi} n^\mu \frac{2}{3} \frac{\alpha}{m} h(\Phi) (\xi_1^2 (\Psi'_1(\Phi))^2 + \xi_2^2 (\Psi'_2(\Phi))^2) d\Phi \end{aligned} \quad (5.7)$$

$$\begin{aligned} &= \tilde{u}_0^\mu - \int_{\phi_0}^{\phi} \frac{1}{\rho_0 m} \left(h(\Phi) e F^{\mu\nu}(\Phi) + \frac{2}{3} \alpha \frac{e}{m} F'^{\mu\nu}(\Phi) \rho_0 \right) \eta_{\alpha\nu} \left(\tilde{u}_0^\alpha \right. \\ &\quad \left. - \frac{1}{\rho_0 m} (f_1^{\alpha\gamma} I_1(\phi) + f_2^{\alpha\gamma} I_2(\phi)) \tilde{u}_{0,\gamma} + \underbrace{\frac{1}{2\rho_0} (h^2(\phi) - 1) n^\alpha}_{\text{mtlp. with } F^{\mu\nu} \text{ gives } =0} \right) d\Phi \\ &\quad + \frac{1}{2\rho_0} (h^2 - 1) n^\mu \end{aligned} \quad (5.8)$$

$$\begin{aligned} &= \tilde{u}_0^\mu - \frac{\tilde{u}_{0,\nu}}{\rho_0 m} \int_{\phi_0}^{\phi} \left(h e f_j^{\mu\nu} \Psi'_j + \frac{2}{3} \alpha \frac{e}{m} f_j^{\mu\nu} \Psi''_j \rho_0 \right) d\Phi + \frac{1}{2\rho_0} (h^2 - 1) n^\mu \\ &\quad + \frac{\eta_{\alpha\nu}}{\rho_0 m} \int_{\phi_0}^{\phi} \left(h e f_j^{\mu\nu} \Psi'_j + \frac{2}{3} \alpha \frac{e}{m} f_j^{\mu\nu} \Psi''_j \rho_0 \right) \frac{1}{\rho_0 m} (f_i^{\alpha\gamma} I_i(\Phi)) \tilde{u}_{0,\gamma} d\Phi \end{aligned} \quad (5.9)$$

$$\begin{aligned} &= \tilde{u}_0^\mu - \frac{\tilde{u}_{0,\nu}}{\rho_0 m} e f_j^{\mu\nu} \int_{\phi_0}^{\phi} I'_j d\Phi + \frac{1}{2\rho_0} (h^2 - 1) n^\mu \\ &\quad + \frac{e^2}{m^2} \frac{1}{\rho_0^2} \underbrace{\eta_{\alpha\nu} f_j^{\mu\nu} f_i^{\alpha\gamma} \tilde{u}_{0,\gamma}}_{=-a_i^2 \delta_{ij} n^\mu n^\gamma \tilde{u}_{0,\gamma}} \int_{\phi_0}^{\phi} I'_j(\Phi) I_i(\Phi) d\Phi \end{aligned} \quad (5.10)$$

$$\begin{aligned} &= \tilde{u}_0^\mu - \frac{e}{\rho_0 m} (f_1^{\mu\nu} I_1 + f_2^{\mu\nu} I_2) \tilde{u}_{0,\nu} + \frac{1}{2\rho_0} (h^2 - 1) n^\mu \\ &\quad + \frac{n^\mu}{\rho_0} \int_{\phi_0}^{\phi} (\xi_1^2 I'_1 I_1 + \xi_2^2 I'_2 I_2) d\Phi \end{aligned} \quad (5.11)$$

$$\begin{aligned} &= \tilde{u}_0^\mu - \frac{e}{\rho_0 m} (f_1^{\mu\nu} I_1(\phi) + f_2^{\mu\nu} I_2(\phi)) \tilde{u}_{0,\nu} + \frac{1}{2\rho_0} (h^2(\phi) - 1) n^\mu \\ &\quad + \frac{1}{2\rho_0} (\xi_1^2 I_1^2(\phi) + \xi_2^2 I_2^2(\phi)) n^\mu, \end{aligned} \quad (5.12)$$

with the relation for the integral analogue to (5.6) but with the relation $I_j(\phi_0) = 0$

$$\int_{\phi_0}^{\phi} I'_j I_j d\Phi = - \int_{\phi_0}^{\phi} I'_j I_j d\Phi + I_j^2(\phi) - I_j^2(\phi_0) = \frac{I_j^2(\phi)}{2}. \quad (5.13)$$

The iteration can be stopped at this point because this is already the exact solution. Putting $\gamma_\nu^{[2]}$ into the integral of $\gamma^{[3]\mu}(\phi)$ one can see that the last term of $\gamma_\nu^{[2]}$ does not contribute because it goes to zero after multiplication with the electromagnetic field tensor $n_\nu F^{\mu\nu} = n_\nu f_j^{\mu\nu} \Psi'_j = 0$ and one is left with the same integral as before.

5.2 Picard iteration for the semiclassical solution

The basic structure is the same as for the classical case but the differential equation is slightly different. It will be solved by picard iteration [20] similar to above where the starting value is $\gamma^{[0]\mu}(\phi) = \tilde{u}_0^\mu$. For $k = 1$ one finds

$$\begin{aligned} \gamma^{[1]\mu}(\phi) &= \tilde{u}_0^\mu - \int_{\phi_0}^{\phi} \frac{\gamma^{[0]\alpha} \eta_{\alpha\nu}}{m\rho_0} \left(\tilde{h}(\Phi) e \frac{\tilde{F}^{\mu\nu}(\Phi)}{\sqrt{g(\Phi)}} \right) d\Phi \\ &\quad + \int_{\phi_0}^{\phi} n^\mu \frac{2}{3} \frac{\alpha}{m} \tilde{h}(\Phi) (\xi_1^2 (\tilde{\Psi}'_1(\Phi))^2 + \xi_2^2 (\tilde{\Psi}'_2(\Phi))^2) d\Phi \end{aligned} \quad (5.14)$$

$$= \tilde{u}_0^\mu - \frac{\tilde{u}_{0,\nu} e}{\rho_0 m} \int_{\phi_0}^{\phi} \tilde{h}(\Phi) f_j^{\mu\nu} \frac{\tilde{\Psi}'_j(\Phi)}{\sqrt{g(\Phi)}} d\Phi + \int_{\phi_0}^{\phi} \frac{n^\mu}{\rho_0} \tilde{h}(\Phi) \tilde{h}'(\Phi) d\Phi \quad (5.15)$$

$$= \tilde{u}_0^\mu - \frac{1}{\rho_0} \frac{e}{m} f_j^{\mu\nu} \tilde{I}_j(\phi) \tilde{u}_{0,\nu} + \frac{1}{2\rho_0} (\tilde{h}^2(\phi) - 1) n^\mu, \quad (5.16)$$

where Einstein notation for $i, j = \{1, 2\}$ is used and the $\tilde{I}_j(\phi)$ in this case being

$$\tilde{I}_j(\phi) \equiv \int_{\phi_0}^{\phi} \tilde{h}(\Phi) \frac{\tilde{\Psi}'_j(\Phi)}{\sqrt{g(\Phi)}} d\Phi. \quad (5.17)$$

For the next step $k = 2$ one finds

$$\begin{aligned} \gamma^{[2]\mu}(\phi) &= \tilde{u}_0^\mu - \int_{\phi_0}^{\phi} \frac{e}{\rho_0 m} \left(\tilde{h}(\Phi) \frac{\tilde{F}^{\mu\nu}(\Phi)}{\sqrt{g(\Phi)}} \right) \eta_{\alpha\nu} \gamma^{[1]\alpha}(\Phi) d\Phi \\ &\quad + \int_{\phi_0}^{\phi} n^\mu \frac{2}{3} \frac{\alpha}{m} \tilde{h}(\Phi) (\xi_1^2 (\tilde{\Psi}'_1(\Phi))^2 + \xi_2^2 (\tilde{\Psi}'_2(\Phi))^2) d\Phi \end{aligned} \quad (5.18)$$

$$\begin{aligned} &= \tilde{u}_0^\mu - \frac{e}{\rho_0 m} \int_{\phi_0}^{\phi} \tilde{h}(\Phi) \frac{f_i^{\mu\nu} \tilde{\Psi}'_i(\Phi)}{\sqrt{g(\Phi)}} \eta_{\alpha\nu} \left(\tilde{u}_0^\alpha - \frac{e}{\rho_0 m} f_j^{\alpha\beta} \tilde{I}_j(\Phi) \tilde{u}_{0,\beta} \right. \\ &\quad \left. + \frac{1}{2\rho_0} (\tilde{h}^2(\Phi) - 1) n^\alpha \right) d\Phi + \frac{1}{2\rho_0} (\tilde{h}^2(\phi) - 1) n^\mu \end{aligned} \quad (5.19)$$

$$\begin{aligned} &= \tilde{u}_0^\mu - \frac{\tilde{u}_{0,\nu} e}{\rho_0 m} f_j^{\mu\nu} \tilde{I}_j(\phi) - \frac{1}{\rho_0^2} \frac{e^2}{m^2} f_i^{\mu\nu} f_j^{\alpha\beta} \eta_{\alpha\nu} \int_{\phi_0}^{\phi} \tilde{I}'_i(\Phi) \tilde{I}_j(\Phi) d\Phi \\ &\quad + \frac{1}{2\rho_0} (\tilde{h}^2(\phi) - 1) n^\mu \end{aligned} \quad (5.20)$$

$$\begin{aligned} &= \tilde{u}_0^\mu - \frac{e}{\rho_0 m} (f_1^{\mu\nu} \tilde{I}_1(\phi) + f_2^{\mu\nu} \tilde{I}_2(\phi)) \tilde{u}_{0,\nu} + \frac{1}{2\rho_0} (\tilde{h}^2(\phi) - 1) n^\mu \\ &\quad + \frac{1}{2\rho_0} (\xi_1^2 \tilde{I}_1^2(\phi) + \xi_2^2 \tilde{I}_2^2(\phi)) n^\mu. \end{aligned} \quad (5.21)$$

With the same argumentation as for the classical solution, this is the exact solution.

5.3 Identities and integrals

a) Identity for total differentials and derivatives

$$-\frac{d^2\phi}{ds^2} = \left(\frac{d\phi}{ds}\right)^3 \frac{d^2s}{d\phi^2} = \left(\frac{d\phi}{ds}\right)^3 \left(\frac{ds}{d\phi} \frac{d}{ds} \frac{ds}{d\phi}\right) = \left(\frac{d\phi}{ds}\right)^2 \left(\frac{d}{ds} \frac{ds}{d\phi}\right) \quad (5.22)$$

$$= \frac{d}{ds} \left(\frac{ds}{d\phi} \left(\frac{d\phi}{ds}\right)^2\right) - \frac{ds}{d\phi} \left(\frac{d}{ds} \left(\frac{d\phi}{ds}\right)^2\right) \quad (5.23)$$

$$= \frac{d^2\phi}{ds^2} - 2\frac{d^2\phi}{ds^2}. \quad (5.24)$$

b) Integral over a closed period

$$\int_0^{2\pi} e^{iax} e^{ibx} dx = 0, \quad (5.25)$$

when $a + b = \text{integers} \setminus \{0\}$.

c) Euler representation of the trigonometric function (\sin^4)

$$\sin^4(x) = \left(-\frac{1}{4} (e^{2ix} + e^{-2ix} - 2)\right)^2 = \frac{1}{16} (e^{4ix} + e^{-4ix} + 6 - 4e^{2ix} - 4e^{-2ix}). \quad (5.26)$$

d) Approximate solution of a double integral for large, positive integers N

$$\begin{aligned} & \int_0^{2\pi N} \sin^2\left(\frac{x}{2N}\right) \sin(nx + a) dx \int_0^x \sin^4\left(\frac{y}{2N}\right) \cos(ny + b) dy \\ & \approx N\pi \cos(a - b) \frac{5}{16} \cdot \frac{1}{n}, \end{aligned} \quad (5.27)$$

where $n = \text{integers}$ and a, b are real values.

6 Bibliography

- [1] V. Yanovsky, V. Chvykov, G. Kalinchenko, P. Rousseau, T. Planchon, T. Matsuoka, A. Maksimchuk, J. Nees, G. Cheriaux, G. Mourou, and K. Krushelnick. Ultra-high intensity- 300-tw laser at 0.1 hz repetition rate. *Opt. Express*, 16(3):2109–2114, Feb 2008. doi: 10.1364/OE.16.002109. URL <http://www.opticsexpress.org/abstract.cfm?URI=oe-16-3-2109>.
- [2] Taken from the APOLLON homepage. URL <https://apollonlaserfacility.cnrs.fr/en/home/>.
- [3] Taken from the ELI homepage. URL <https://eli-laser.eu/>.
- [4] J. D. Jackson. *Electrodynamics, Classical*. American Cancer Society, 2003. ISBN 9783527600434. doi: <https://doi.org/10.1002/3527600434.eap109>. URL <https://onlinelibrary.wiley.com/doi/abs/10.1002/3527600434.eap109>.
- [5] Max Abraham. *Theorie der Elektrizität, Vol. 2*. (Teubner, Leipzig, 1908).
- [6] L. Landau and E. Lifschitz. *The Classical Theory of Fields*. (Elsevier, Oxford, 1975).
- [7] Paul Adrien Maurice Dirac. Classical theory of radiating electrons. *Proceedings of the Royal Society of London. Series A. Mathematical and Physical Sciences*, 167(929):148–169, 1938. doi: 10.1098/rspa.1938.0124. URL <https://royalsocietypublishing.org/doi/abs/10.1098/rspa.1938.0124>.
- [8] Ernest J. Moniz and D. H. Sharp. Radiation reaction in nonrelativistic quantum electrodynamics. *Physical Review. D, Particles Fields*, 15(10), 5 1977. ISSN 0556-2821. doi: 10.1103/PhysRevD.15.2850. URL <https://www.osti.gov/biblio/7259064>.
- [9] Dieter Gromes. Where the lorentz-abraham-dirac equation for the radiation reaction force fails, and why the “proofs” break down. July 2005. URL <https://www.thphys.uni-heidelberg.de/~gromes/LAD.pdf>.

-
- [10] Freeman Dyson. *Dyson Quantenfeldtheorie*. ISBN 978-3-642-37677-1. Springer-Verlag Berlin Heidelberg, 2014.
- [11] V. I. Ritus. Quantum effects of the interaction of elementary particles with an intense electromagnetic field. *Journal of Soviet Laser Research*, 6(5):497–617, Sep 1985. ISSN 1573-8760. doi: 10.1007/BF01120220. URL <https://doi.org/10.1007/BF01120220>.
- [12] A. Di Piazza. Exact solution of the Landau-Lifshitz equation in a plane wave. *Letters in Mathematical Physics*, 83(3):305–313, Mar 2008. ISSN 1573-0530. doi: 10.1007/s11005-008-0228-9. URL <https://doi.org/10.1007/s11005-008-0228-9>.
- [13] Matteo Tamburini, Christoph H. Keitel, and Antonino Di Piazza. Electron dynamics controlled via self-interaction. *Physical Review E*, 89(2), Feb 2014. ISSN 1550-2376. doi: 10.1103/PhysRevE.89.021201. URL <http://dx.doi.org/10.1103/PhysRevE.89.021201>.
- [14] V. N. Baier, V. M. Katkov, and V. M. Strakhovenko. *Electromagnetic Processes at High Energies in Oriented Single Crystals*. World Scientific, Singapore, 1998. doi: 10.1142/2216. URL <https://www.worldscientific.com/doi/abs/10.1142/2216>.
- [15] K. Poder, M. Tamburini, G. Sarri, A. Di Piazza, S. Kuschel, C. D. Baird, K. Behm, S. Bohlen, J. M. Cole, D. J. Corvan, and et al. Experimental signatures of the quantum nature of radiation reaction in the field of an ultraintense laser. *Physical Review X*, 8(3), Jul 2018. ISSN 2160-3308. doi: 10.1103/PhysRevX.8.031004. URL <http://dx.doi.org/10.1103/PhysRevX.8.031004>.
- [16] M. Tamburini, F. Pegoraro, A. Di Piazza, C. H. Keitel, and A. Macchi. Radiation reaction effects on radiation pressure acceleration. *New Journal of Physics*, 12(12):123005, Dec 2010. ISSN 1367-2630. doi: 10.1088/1367-2630/12/12/123005. URL <http://dx.doi.org/10.1088/1367-2630/12/12/123005>.
- [17] N. Neitz and A. Di Piazza. Stochasticity effects in quantum radiation reaction. *Phys. Rev. Lett.*, 111:054802, Aug 2013. doi: 10.1103/PhysRevLett.111.054802. URL <https://link.aps.org/doi/10.1103/PhysRevLett.111.054802>.
- [18] Yousef I. Salamin and Christoph H. Keitel. Electron Acceleration by a Tightly Focused Laser Beam. , 88(9):095005, March 2002. doi: 10.1103/PhysRevLett.88.095005.

-
- [19] Kirk T. McDonald. A relativistic electron can't extract net energy from a long laser pulse. Aug 1997. ISSN NJ 08544. URL <https://physics.princeton.edu/~mcdonald/examples/gaussian2.pdf>.
- [20] Ina Kersten. *Gewöhnliche Differenzialgleichungen*. ISBN 978-3-86395-221-1. Universitätsverlag Göttingen, 2015.

7 Acknowledgements

I want to thank Prof. Dr. Christoph Keitel for giving me the opportunity to write my thesis in his division at the MPIK. Also I want to thank Kevin Zink for the IT-support and Sibel Babacan for helping me with various organisational problems.

At most I want to thank Dr. Matteo Tamburini, who has been my supervisor during the last months, for steadily answering my questions, for great help and very friendly support.

Further I want to thank my family, my friends and my girlfriend for keeping me in a good mood during several isolated winter months.

Erklärung:

Ich versichere, dass ich diese Arbeit selbstständig verfasst habe und keine anderen als die angegebenen Quellen und Hilfsmittel benutzt habe.

Heidelberg, den

26.3.2021 Bastian Brunner